Available online at www.sciencedirect.com

ScienceDirect

Journal of the Franklin Institute 360 (2023) 3520–3544

www.elsevier.com/locate/jfranklin

Trajectory tracking of a quadrotor using extend state observer based U-model enhanced double sliding mode control

Ruobing Li*, Quanmin Zhu, Hamidreza Nemati, Xicai Yue, Pritesh Narayan

Department of Engineering Design and Mathematics, University of the West of England, Frenchy Campus, Coldharbour Lane Bristol, BS16 1QY, UK

Received 31 May 2022; received in revised form 5 October 2022; accepted 15 November 2022
Available online 26 November 2022

Abstract

This paper develops a novel U-model enhanced double sliding mode controller (UDSMC) for a quadrotor based on multiple-input and multiple-output extended-state-observer (MIMO-ESO). UDSMC is designed using Lyapunov synthesis and Hurwitz stability to not only cancel the complex dynamics and nonlinearity, but also stabilize the uncertainty and external disturbance of the underlying quadrotors. MIMO-ESO is designed to estimate the unmeasurable velocities which can reduce the impact of sensor measurement errors in practice. The difficulties associated with quadrotor velocity's measurement disturbances and uncertain aerodynamics are successfully addressed in this control design. Rigorous theoretical analysis has been carried out to determine whether the proposed control system can achieve stable trajectory tracking performance, and a comparative real-time experimental study has also been carried out to verify the better effectiveness of the proposed control system than the built-in PID control system.

* Corresponding author.
E-mail addresses: ruobing2.li@live.uwe.ac.uk (R. Li), quan.zhu@uwe.ac.uk (Q. Zhu), Hamidreza.Nemati@uwe.ac.uk (H. Nemati), alex.yue@uwe.ac.uk (X. Yue), pritesh.narayan@uwe.ac.uk (P. Narayan).

https://doi.org/10.1016/j.jfranklin.2022.11.036

1. Introduction

The quadrotor has all advantages of Vertical Take-Off and Landing (VTOL) aircraft along with a smaller size, more payload capability, greater hover stability and greater manoeuvrability. Compared with conventional aircraft, quadrotor UAV has a simpler mechanical structure and easier take-off conditions. Nowadays, particularly in academia and the industry, along with the research and development communities, there has been a growth of interest in UAVs [1–3]. Probably, the feasibility of effectively performing various tasks with a wide range of applications like courier delivery, spraying of pesticides, aerial photography, surveying and mapping, wildfire surveillance, search and rescue missions, and several others, could have whetted this popularity [3]. Besides the endurance, cost, and size of the unmanned aircraft being highly attractive, the possibility of keeping human pilots out of danger (human capacity or aircraft failure) could be a matter of high concern [1]. Nevertheless, in the case of practical flight missions, there could be the risk of the stability of the aircraft being degraded sensitively by obstacles in the air, sudden change of command, and turbulent changes in weather conditions. Hence, in the flight process, it is crucial to have a flight controller design that could provide the aircraft with a robust and accurate control.

As a result of the quadrotor structures with the existing six-state outputs, which include the angles and the robot positions in such a manner that there would be only four rotors available for control inputs, the quadrotor UAV is known as an underactuated system. The rotational and transitional movements of the quadrotor are made possible by the speed variations of the rotors. Overall, basic control target of the quadrotors involves the control of the altitude and the attitude for the quadrotor to continue holding the same position in the specified location [4]. There could be several issues of challenges in the control of the UAVs, such as disturbances from the atmosphere and input constraints, nonlinear components, time-varying states and delays, un-modelled dynamics, uncertainty of the parameters, under-actuation, coupled states, open-loop instability, and the MIMO structure [5–6]. Thus, for the control of the quadrotors several control schemes have been applied. The literature reported the outcomes of the methods that were non-adaptive like the state feedback [7], Proportional–Integral–Derivative (PID) [8], and the Linear-Quadratic-Regulator (LQR) [9].

Nonetheless, robust and adaptive methods of control would display a better control performance because quadrotor system dynamics are nonlinear in addition to being time-varying. The Sliding Mode Control (SMC) is a conventional method of control for dealing with the bounded external disturbances, the nonlinearities, the properties of time-variations, and other uncertainties [10]. Zheng and Xiong [11] developed an integrated approach to quadrotor attitude and position tracking control, in which the dynamics model is divided into underactuated and fully actuated subsystems. To compensate for faults in quadrotor motor actuators, the SMC observer applies linear parameter changes [12]. While in case of quad-rotor systems that are under-actuated and uncertain, it is proposed to have a system for tracking and stability control according to the technique of the SMC [13]. Nevertheless, in the pertinent paper, a fully actuated dynamic model of the quadrotor was not considered suitable for our application. Initially, the continuous-time quadrotor dynamic model was converted to a discrete-time model [14]. Later, to control the tracking and stability of the modified quadrotor model, discrete SMC was proposed. Mofid and Mobayen [15] studied the efficiency of adaptive SMC under uncertain model parameters, Lyapunov's proof method also exhibits its finite-time stability. The proposed method is evaluated by simulation.

Nonetheless, many issues still remain to be resolved in quadrotor control. Most of the existing quadrotor controllers are designed based on a simplified dynamic model that ignores its complex nonlinearities and disturbances. amongst them, the decoupling problems caused by the complex transformation between the frame systems is important, which directly increases the design difficulty of quadrotor position controller [16,17]. [18] proposed a nonlinear decoupling controller using surface control and disturbance observer, but the radical term that appears in the denominator of the decoupling algorithm will undoubtedly limit its application. [17] improves the decoupling method based on [18]to achieve position tracking, which reduces the trigonometric computation, but it has the same problem as [18], the radical item will limit its application. [19] only decouples yaw dynamics from other dynamics. [20] proposed a fuzzy logic controller to decouple the position and attitude of the quadrotor, but the design of its inner loop attitude controller ignored nonlinear dynamics. Additionally, majority of the early works have evaluated control methods through simulations [21–25], only certain works could establish real-time control on quadrotors [26–28]. There are significant differences between real-time experiments and simulations. In most simulation studies, the control signal is usually considered to be the torque or force produced by the rotor. Therefore, rotors with dynamic models are ignored. Furthermore, aerodynamic perturbations, matrix asymmetry of the moment of inertia, mass imbalance, effects of wind and eddy currents, besides the air-friction and that between the air and the drone were also neglected. In addition to all the above factors, another crucial aspect is the measurement of velocity sensor noise.

Considering the above real-time experimental results, the experimental test of QBall2 by Quanser in [26] has a spherical outer protective shell, its diameter is about twice the length of the quadrotor. While protecting the fuselage, this kind of protective shell will also increase its mass, which will increase the moment generated when the quadrotor's attitude changes and result in affecting the stability design of the control system as well as its test of the anti-disturbance ability of the flight controller. The quadrotor in [28] is mounted on a passive mechanical suspension to reduce the effect of rotor vibration, and at the same time limit the small angular changes of the aircraft. [27] requires a large amount of actual flight data to train reinforcement learning models, which is therefore time and computationally expensive. In this study, a MIMO-ESO is designed to estimate the disturbance and unmeasured velocities. The Lyapunov analysis is used to prove the convergence boundary of ESO estimated error. For tracking a time-varying trajectory of the quadrotor stably, the Double Sliding Mode Control (DSMC) based inverter (for robustness and nonlinear dynamic cancellation) and a U-controller (for the control performance specification), are included in the control system. The Lyapunov analysis proved the stability of the proposed control system, and the Hurwitz stability theory was applied for designing the related sliding manifolds coefficients. The control efficiency is tested and evaluated by real-time experimental Parrot Minidrone.

Summarily, the major contributions of this paper are:

1) To the authors' knowledge, this is the first study to apply U-control method to a real-time application (quadrotor control).
2) Proposing a quadrotor decoupling algorithm, using an indirect control strategy (position control by controlling the angle) turns the original underactuated system into a fully actuated system. This decoupling algorithm is implemented by DSMC method, which avoid the square root calculation in [17,18].
3) Based on Lyapunov analysis, presenting a MIMO-ESO for unmeasured velocities estimation and a robust framework for flight control of quadrotors based on the ESO UDSMC method.

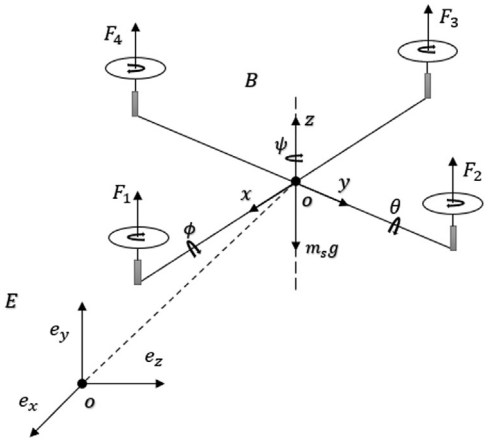

Fig. 1. Quadrotor aircraft framework.

4) Expand the SISO implementation and application of the UDSMI [29] into MIMO systems with obvious progression in integrating SISO UDSMC and MIMO UDSMC plus decoupling.
5) Comparative experimental studies with the built-in PID controller (come from the product) and SMC method (advanced control algorithm) are involved to show the efficiency of the proposed controller.

The remaining portion of this paper has been arranged as follows. Section 2 introduces the dynamical model of the quadrotor and control problems for follow up development. In Section 3, the MIMO-ESO is derived to estimate the unmeasured quadrotor's velocities. Section 4 presents the UDSMC method firstly, then comes with its quadrotor flight controller design procedures, coefficients designed principle and stability analysis. Also, it proposes a new decoupling algorithm for the quadrotor flight operation. Section 5 presents the experimental bench tests, which shows the experimental setup procedure, design parameters of the involved control methods and experiment results to compare to demonstrate the efficiency of the proposed control system. Section 6 concludes the study.

2. Dynamic description and problem statement

2.1. Quadrotor dynamic model

This study considers and tests followed quadrotor motion control: (1) Roll and pitch control: change the output power of the neighbouring motors to tilt; (2) Yaw control: change the output power of the opposing motors to generate unbalanced torque; (3) Horizontal movement control, the roll or pitch of the vehicle will generate a horizontal component of the rotor lift, thereby realizing the horizontal movement of the quadrotor; (4) Vertical movement control: increase or decrease the output power of all motors by the same account; (5) Hover Control: make the output power of all motors the same and the lifting force they generate is equal to the gravity [1].

Fig. 1 shows the quadrotor framework and its dynamical model which is established by the body-frame $B(Oxyz)$ and the earth-frame $E(Oxyz)$. In quadrotor position control, the compensation of the rotation is necessary and obtained from the rotation matrix $R: E \rightarrow B$:

$$\boldsymbol{R} = R(\phi, \theta, \psi) = R(z, \psi)R(y, \theta)R(x, \phi)$$

$$R(z, \psi) = \begin{bmatrix} cos\ \psi & -\sin\psi & 0 \\ \sin\psi & cos\ \psi & 0 \\ 0 & 0 & 1 \end{bmatrix}$$

$$R(y, \theta) = \begin{bmatrix} cos\ \theta & 0 & \sin\theta \\ 0 & 1 & 0 \\ -\sin\theta & 0 & cos\ \theta \end{bmatrix}$$

$$R(x, \phi) = \begin{bmatrix} 1 & 0 & 0 \\ 0 & cos\ \phi & -\sin\phi \\ 0 & \sin\phi & cos\ \phi \end{bmatrix} \tag{1}$$

where roll ϕ, pitch θ and yaw ψ angles are quadrotor orientation in the body frames. Then it comes from (1):

$$\boldsymbol{R} = \begin{bmatrix} C_\psi C_\theta & C_\psi S_\theta S_\phi - S_\psi C_\phi & C_\psi S_\theta C_\phi + S_\psi S_\phi \\ S_\psi C_\theta & S_\psi S_\theta S_\phi + C_\psi C_\phi & S_\psi S_\theta C_\phi - C_\psi S_\phi \\ -S_\theta & C_\theta S_\phi & C_\theta C_\phi \end{bmatrix} \tag{2}$$

where S denotes $sin(\cdot)$ and C denotes $cos(\cdot)$. The translational kinematic equations are attained by:

$$\boldsymbol{v_e} = \boldsymbol{R} \cdot \boldsymbol{v_b} \tag{3}$$

where $\boldsymbol{v_e} = [u_0,\ v_0,\ w_0]^T$ and $\boldsymbol{v_b} = [u_b,\ v_b,\ w_b]^T$ are quadrotor's linear velocities in the earth-frame $E(Oxyz)$ and body-frame $B(Oxyz)$, respectively. This study considers the following assumptions to simplify the dynamics modelling complexity [1]:

1) The structure of quadrotor is rigid and symmetrical.
2) The propeller that produces lift is rigid.
3) The air drag forces are proportional to the propellers' speed.

Under these assumptions, the quadrotor flight dynamics can be presented by the flight dynamics of a rigid body under the aerodynamic forces and moments generated by the rotation of the propeller. Then the translational motions and rotational motions kinetic equations of quadrotor can be described as:

$$\begin{cases} m_s\ddot{\boldsymbol{P}} = \boldsymbol{F_f} + \boldsymbol{F_d} + \boldsymbol{F_g} \\ J\ddot{\boldsymbol{\Theta}} = -\dot{\boldsymbol{\Theta}} \times \left(\boldsymbol{J}\dot{\boldsymbol{\Theta}}\right) + \boldsymbol{\Gamma_f} - \boldsymbol{\Gamma_a} - \boldsymbol{\Gamma_g} \end{cases} \tag{4}$$

where m_s is the total mass of the quadrotor; vector $\boldsymbol{P} = [x,\ y,\ z]^T$ presents the quadrotor position; $\boldsymbol{F_f} = \boldsymbol{R}_{j,3}\sum_{i=1}^{4} F_i = \boldsymbol{R}_{j,3}K_p\omega_i^2$ presents the composition of forces generated by all rotors with $\boldsymbol{R}_{j,3}$ being the third column of the rotation matrix $\boldsymbol{R}$ in (2) and K_p being a coefficient related to the square of the angular rotor speed ω_i^2, which can be determined by static thrust tests [30]. $\boldsymbol{F_d} = diag(-K_1, -K_2, -K_3)\dot{\boldsymbol{P}}$ presents the composition of the drag forces along $(X,\ Y,\ Z)$ axis with $K_i (i = 1, 2, 3)$ being positive translation air drag coefficients. $\boldsymbol{F_g} = [0, 0, -m_s g]^T$ presents the gravity force acting on the centre of mass

with g being gravitational acceleration. Euler angles vector $\boldsymbol{\Theta} = [\phi, \theta, \psi]^T$ donates quadrotor orientation. $\boldsymbol{J} = diag(I_x,\ I_y, I_z)\ \in \mathbb{R}^{3\times 3}$ is a positive definite symmetric inertia matrix of the quadrotor with $I_i (i = x, y, z)$ being the inertial moment in the body-frame $B(Oxyz)$. $\boldsymbol{\Gamma_a} = diag(K_{ax}, K_{ay}, K_{az})\dot{\boldsymbol{\Theta}}$ presents the composition of aerodynamic resistance torque with K_{ax}, K_{ay} and K_{az} being the coefficients of aerodynamic resistance. $\boldsymbol{\Gamma_f}$ is the moment generated by the rotation of the propeller for the quadrotor's fixed frame and $\boldsymbol{\Gamma_g}$ is the composition of torques due to the gyroscopic effects [30], these forces are described by:

$$\boldsymbol{\Gamma_f} = \begin{pmatrix} l(F_3 - F_1) \\ l(F_2 - F_4) \\ \omega_1^2 - \omega_2^2 + \omega_3^2 - \omega_4^2 \end{pmatrix} = \begin{pmatrix} lK_p\left(\omega_3^2 - \omega_1^2\right) \\ lK_p\left(\omega_4^2 - \omega_2^2\right) \\ \omega_1^2 - \omega_2^2 + \omega_3^2 - \omega_4^2 \end{pmatrix} \tag{5}$$

$$\boldsymbol{\Gamma_g} = \sum_{i=1}^{4} J_r \begin{pmatrix} 0 \\ 0 \\ (-1)^{i+1}\omega_i \end{pmatrix} \dot{\boldsymbol{\Theta}} \tag{6}$$

where l is the length between the centre of mass of the quadrotor and the axis of rotation of the propeller, J_r is the rotor inertia along the z axis. The angular velocities $[p,\ q,\ r]^T$ in the body frame can be obtained by transforming the angular velocity $[\dot{\phi},\ \dot{\theta},\ \dot{\psi}]^T$ in the inertial frame as:

$$\begin{pmatrix} p \\ q \\ r \end{pmatrix} = \begin{pmatrix} 1 & 0 & -\sin\theta \\ 0 & \cos\phi & \cos\theta\sin\phi \\ 0 & -\sin\phi & \cos\phi\cos\theta \end{pmatrix} \begin{pmatrix} \dot{\phi} \\ \dot{\theta} \\ \dot{\psi} \end{pmatrix} \tag{7}$$

Therefore, the mathematical dynamics of a quadrotor can be established by:

$$\begin{cases} \ddot{x} = \frac{1}{m_s}(cos\ \psi \sin\theta cos\ \phi + \ \sin\phi \sin\psi)u_1 - \frac{1}{m_s}K_1\dot{x} \\ \ddot{y} = \frac{1}{m_s}(\sin\psi \sin\theta cos\ \phi - cos\ \psi \sin\phi)u_1 - \frac{1}{m_s}K_2\dot{y} \\ \ddot{z} = \frac{1}{m_s}(cos\ \theta cos\ \phi)u_1 - g - \frac{1}{m_s}K_3\dot{z} \end{cases} \tag{8}$$

$$\begin{cases} \ddot{\phi} = \frac{l}{I_x}\left[\left(I_y - I_z\right)qr - K_{ax}p - J_r q\Omega_r + u_2\right] \\ \ddot{\theta} = \frac{l}{I_y}\left[(I_z - I_x)pr - K_{ay}q + J_r p\Omega_r + u_3\right] \\ \ddot{\psi} = \frac{1}{I_z}\left[\left(I_x - I_y\right)pq - K_{az}r + u_4\right] \end{cases} \tag{9}$$

where $\Omega_r = \omega_1 - \omega_2 + \omega_3 - \omega_4$ presents the total rotor angular velocity, u_1 represents the total thrust acting on the body in the z-axis, u_2 represents the roll torque and u_3 represent the pitch torques; u_4 represents the yaw torque. Rewrite them by the angular velocities as follows:

$$\begin{bmatrix} u_1 \\ u_2 \\ u_3 \\ u_4 \end{bmatrix} = \begin{bmatrix} K_p & K_p & K_p & K_p \\ -lK_p & 0 & lK_p & 0 \\ 0 & lK_p & 0 & -lK_p \\ 1 & -1 & 1 & -1 \end{bmatrix} \begin{bmatrix} \omega_1^2 \\ \omega_2^2 \\ \omega_3^2 \\ \omega_4^2 \end{bmatrix} \tag{10}$$

Let us introduce the following notations for simplicity:

$$\begin{aligned} &\boldsymbol{X}_1 = \boldsymbol{P}, \boldsymbol{X}_2 = \dot{\boldsymbol{P}},\ \boldsymbol{X}_4 = \boldsymbol{\Theta},\ \boldsymbol{X}_5 = \dot{\boldsymbol{\Theta}}, \boldsymbol{F} = \left(\boldsymbol{F_f} + \boldsymbol{F_g}\right)/m_s, \\ &f_2(\boldsymbol{X}_2) = \boldsymbol{F_d}/m_s = (diag(-K_1, -K_2, -K_3)\boldsymbol{X}_2)/m_s, \\ &f_5(\boldsymbol{X}_5) = \boldsymbol{J}^{-1}\left(-\dot{\boldsymbol{\Theta}} \times \left(\boldsymbol{J}\dot{\boldsymbol{\Theta}}\right) - \boldsymbol{\Gamma_a} - \boldsymbol{\Gamma_g}\right) \end{aligned} \tag{11}$$

Then the original translational and rotational models of the quadrotor (8) and (9) can be converted into

$$\begin{cases} \dot{\boldsymbol{X}}_1 = \boldsymbol{X}_2 \\ \dot{\boldsymbol{X}}_2 = f_2(\boldsymbol{X}_2) + F + \boldsymbol{d}_2 \\ \dot{\boldsymbol{X}}_4 = \boldsymbol{X}_5 \\ \dot{\boldsymbol{X}}_5 = f_5(\boldsymbol{X}_5) + \boldsymbol{J}^{-1}\boldsymbol{\Gamma}_f + \boldsymbol{d}_5 \end{cases} \tag{12}$$

where $\boldsymbol{d}_2$ and $\boldsymbol{d}_5$ present lumped disturbances absorbing the uncertainties and external disturbances in the translational and rotational subsystems, respectively, where the uncertainties consist of inaccurate parameters, unmodelled unknown nonlinearities, etc. and the disturbances includes unpredictable environmental variables, sensor measurement noise, etc. The introduction of lumped disturbances can describe the quadrotor model more accurately, which will facilitate the design of MIMO-ESO and controllers.

2.2. Problem statement

According to the dynamical model from (14) to (16), the quadrotor control system can be separated into: a fully actuated subsystem composed of ϕ, θ and ψ and a underactuated subsystem composed of x, y and z. However, in the attitude control of the quadrotor, the changes of the pitch angle θ and roll angle ϕ will cause the drone to tilt, so that the lift force of the rotor generates a horizontal component, then the horizontal movement can be realized. In this case, this study will directly use u_1 to control the quadrotor altitude z, and incidentally realize the x, y position tracking of the quadrotor by controlling the pitch θ and roll ϕ angle. Therefore, the new subsystems implemented by the decoupling algorithm will be separated into: a fully actuated subsystem composed of z and ψ and a underactuated subsystem composed of x, y, ϕ and θ.

Denote by $[x_d,\ y_d,\ z_d]^T$ and $[\phi_d, \theta_d, \psi_d]^T$ the desired positions and attitude angles respectively. The central control problem considered in this study is to design a robust tracking control system including a decoupling algorithm, position and attitude control algorithms to ensure that the quadrotor can follow the desired position and attitude trajectories asymptotically and stably despite the modelling errors and unknown external system disturbances. In other words, the control strategy proposed in this study should ensure the position tracking errors ($e_x = x_d - x$, $e_y = y_d - y$, $e_z = z_d - z$) and the attitude tracking errors ($\phi_x = \phi_d - \phi$, $\theta_y = \theta_d - \theta$, $\psi_z = \psi_d - \psi$) converge to zero.

3. ESO design and analysis

This section introduces the specific MIMO-ESO design process for translational and rotational subsystems. This MIMO-ESO provides not only quadrotor's velocities but also disturbance estimation. According to the ESO design [31], it is necessary to assume $\boldsymbol{d}_2$ and $\boldsymbol{d}_5$ are continuously differentiable and their derivatives $\boldsymbol{h}_3$ and $\boldsymbol{h}_6$ are bounded. Introduce $\boldsymbol{X}_3 = \boldsymbol{d}_2$ and $\boldsymbol{X}_6 = \boldsymbol{d}_5$ for additional state variables, then convert the original translational and rotational models of the quadrotor (12) into:

$$\begin{cases} \dot{\boldsymbol{X}}_1 = \boldsymbol{X}_2 \\ \dot{\boldsymbol{X}}_2 = f_2(\boldsymbol{X}_2) + F + \boldsymbol{X}_3 \\ \dot{\boldsymbol{X}}_3 = \boldsymbol{h}_3 \end{cases} \quad \begin{cases} \dot{\boldsymbol{X}}_4 = \boldsymbol{X}_5 \\ \dot{\boldsymbol{X}}_5 = f_5(\boldsymbol{X}_5) + \boldsymbol{J}^{-1}\boldsymbol{\Gamma}_f + \boldsymbol{X}_6 \\ \dot{\boldsymbol{X}}_6 = \boldsymbol{h}_6 \end{cases} \tag{13}$$

With the definition of $\boldsymbol{X}_T = [\boldsymbol{X}_1 \quad \boldsymbol{X}_2 \quad \boldsymbol{X}_3]^T$ and $\boldsymbol{X}_R = [\boldsymbol{X}_4 \quad \boldsymbol{X}_5 \quad \boldsymbol{X}_6]^T$, system (13) can be covert into:

$$\begin{cases} \dot{\boldsymbol{X}}_T = \boldsymbol{\mathcal{A}}\boldsymbol{X}_T + \boldsymbol{\mathcal{F}}_1(\boldsymbol{X}_T) + \boldsymbol{\mathcal{L}}_2\boldsymbol{F} + \Delta_T \\ \dot{\boldsymbol{X}}_R = \boldsymbol{\mathcal{A}}\boldsymbol{X}_R + \boldsymbol{\mathcal{F}}_2(\boldsymbol{X}_R) + \boldsymbol{\mathcal{L}}_2\left(\boldsymbol{J}^{-1}\boldsymbol{\Gamma}_f\right) + \Delta_R \end{cases} \tag{14}$$

where $\boldsymbol{\mathcal{A}} = \begin{bmatrix} 0 & \boldsymbol{I}_3 & 0 \\ 0 & 0 & \boldsymbol{I}_3 \\ 0 & 0 & 0 \end{bmatrix}$, $\boldsymbol{\mathcal{F}}_1(\boldsymbol{X}_T) = [0 \quad f_2(\boldsymbol{X}_2) \quad 0]^T$, $\boldsymbol{\mathcal{F}}_2(\boldsymbol{X}_R) = [0 \quad f_5(\boldsymbol{X}_5) \quad 0]^T$, $\Delta_T = [0 \quad 0 \quad \boldsymbol{h}_3]^T$, $\Delta_R = [0 \quad 0 \quad \boldsymbol{h}_6]^T$ and $\boldsymbol{\mathcal{L}}_2 = [0 \quad \boldsymbol{I}_3 \quad 0]^T$. $\boldsymbol{I}_i$ presents an $i \times i, i \in \mathbb{R}^+$ identity matrix and $\boldsymbol{0}$ is a zero vector with proper dimensions. Therefore, the MIMO-ESO design based on dynamic modelling information in (11) is:

$$\begin{cases} \dot{\hat{\boldsymbol{X}}}_T = \boldsymbol{\mathcal{A}}\hat{\boldsymbol{X}}_T + \boldsymbol{\mathcal{F}}_1\left(\hat{\boldsymbol{X}}_T\right) + \boldsymbol{\mathcal{L}}_2 F + \boldsymbol{\beta}_1\left(\boldsymbol{X}_1 - \hat{\boldsymbol{X}}_1\right) \\ \dot{\hat{\boldsymbol{X}}}_R = \boldsymbol{\mathcal{A}}\hat{\boldsymbol{X}}_R + \boldsymbol{\mathcal{F}}_2\left(\hat{\boldsymbol{X}}_R\right) + \boldsymbol{\mathcal{L}}_2\left(\boldsymbol{J}^{-1}\boldsymbol{\Gamma}_f\right) + \boldsymbol{\beta}_2\left(\boldsymbol{X}_4 - \hat{\boldsymbol{X}}_4\right) \end{cases} \tag{15}$$

where $\hat{\boldsymbol{X}}_T = [\hat{\boldsymbol{X}}_1 \quad \hat{\boldsymbol{X}}_2 \quad \hat{\boldsymbol{X}}_3]^T$ and $\hat{\boldsymbol{X}}_R = [\hat{\boldsymbol{X}}_4 \quad \hat{\boldsymbol{X}}_5 \quad \hat{\boldsymbol{X}}_6]^T$ are the estimated state variable matrix, $\boldsymbol{\mathcal{F}}_1(\hat{\boldsymbol{X}}_T) = [0 \quad f_2(\hat{\boldsymbol{X}}_2) \quad 0]^T$, $\boldsymbol{\mathcal{F}}_2(\hat{\boldsymbol{X}}_R) = [0 \quad f_5(\hat{\boldsymbol{X}}_5) \quad 0]^T$ $\boldsymbol{\beta}_1$ and $\boldsymbol{\beta}_2$ are the observer gain matrices with $\boldsymbol{\beta}_1 = [3\omega_1 \cdot \boldsymbol{I}_3 \quad 3\omega_1^2 \cdot \boldsymbol{I}_3 \quad \omega_1^3 \cdot \boldsymbol{I}_3]^T$ and $\boldsymbol{\beta}_2 = [3\omega_2 \cdot \boldsymbol{I}_3 \quad 3\omega_2^2 \cdot \boldsymbol{I}_3 \quad \omega_2^3 \cdot \boldsymbol{I}_3]^T$. The parameters $\omega_1, \omega_2 \in \mathbb{R}^+$ are the only tuning parameters presenting the observer bandwidths. Then introduce the estimation errors as $\tilde{\boldsymbol{X}}_T = \boldsymbol{X}_T - \hat{\boldsymbol{X}}_T = [\tilde{\boldsymbol{X}}_1 \quad \tilde{\boldsymbol{X}}_2 \quad \tilde{\boldsymbol{X}}_3]^T$ and $\tilde{\boldsymbol{X}}_R = \boldsymbol{X}_R - \hat{\boldsymbol{X}}_R = [\tilde{\boldsymbol{X}}_4 \quad \tilde{\boldsymbol{X}}_5 \quad \tilde{\boldsymbol{X}}_6]^T$, respectively. Their scaled estimation errors are defined as $\boldsymbol{\mathcal{Q}}_T = [\boldsymbol{\mathcal{Q}}_1 \quad \boldsymbol{\mathcal{Q}}_2 \quad \boldsymbol{\mathcal{Q}}_3]^T = [\tilde{\boldsymbol{X}}_1 \quad \tilde{\boldsymbol{X}}_2/\omega_1 \quad \tilde{\boldsymbol{X}}_3/\omega_1^2]^T$ and $\boldsymbol{\mathcal{Q}}_R = [\boldsymbol{\mathcal{Q}}_4 \quad \boldsymbol{\mathcal{Q}}_5 \quad \boldsymbol{\mathcal{Q}}_6]^T = [\tilde{\boldsymbol{X}}_4 \quad \tilde{\boldsymbol{X}}_5/\omega_2 \quad \tilde{\boldsymbol{X}}_6/\omega_2^2]^T$. Thus, the scaled estimation errors are:

$$\begin{cases} \dot{\boldsymbol{\mathcal{Q}}}_T = \omega_1 \cdot \boldsymbol{\mathcal{A}}_1\boldsymbol{\mathcal{Q}}_T + \boldsymbol{\mathcal{L}}_2\left(f_2(\boldsymbol{X}_2) - f_2\left(\hat{\boldsymbol{X}}_2\right)\right) \cdot \omega_1^{-1} + \boldsymbol{\mathcal{L}}_3\boldsymbol{h}_3 \cdot \omega_1^{-2} \\ \dot{\boldsymbol{\mathcal{Q}}}_R = \omega_1 \cdot \boldsymbol{\mathcal{A}}_1\boldsymbol{\mathcal{Q}}_R + \boldsymbol{\mathcal{L}}_2\left(f_5(\boldsymbol{X}_5) - f_5\left(\hat{\boldsymbol{X}}_5\right)\right) \cdot \omega_2^{-1} + \boldsymbol{\mathcal{L}}_3\boldsymbol{h}_6 \cdot \omega_2^{-2} \end{cases} \tag{16}$$

with $\boldsymbol{\mathcal{A}}_1 = \begin{bmatrix} -3 \cdot \boldsymbol{I}_3 & \boldsymbol{I}_3 & 0 \\ -3 \cdot \boldsymbol{I}_3 & 0 & \boldsymbol{I}_3 \\ -\boldsymbol{I}_3 & 0 & 0 \end{bmatrix}$ and $\boldsymbol{\mathcal{L}}_3 = [0 \quad 0 \quad \boldsymbol{I}_3]^T$

Assumption 1. The derivatives of the lumped disturbances satisfy $||\boldsymbol{h}_3|| \leq \varepsilon_1$ *and* $||\boldsymbol{h}_6|| \leq \varepsilon_2$ with $\varepsilon_1, \varepsilon_3 > 0$. Functions f_2 and f_5 belong to C^2 (with 2 continuous derivatives) and are globally Lipschitz with respect to $\boldsymbol{X}_2$ and $\boldsymbol{X}_5$ with $c_1, c_2 \in \mathbb{R}^+$, that is,

$$\begin{cases} \|f_2(\boldsymbol{X}_2) - f_2\left(\hat{\boldsymbol{X}}_2\right)\| \leq c_1\|\boldsymbol{X}_2 - \hat{\boldsymbol{X}}_2\| = c_1\omega_1\|\boldsymbol{\mathcal{Q}}_2\| \leq c_1\omega_1\|\boldsymbol{\mathcal{Q}}_T\| \\ \|f_5(\boldsymbol{X}_5) - f_5\left(\hat{\boldsymbol{X}}_5\right)\| \leq c_2\|\boldsymbol{X}_5 - \hat{\boldsymbol{X}}_5\| = c_2\omega_2\|\boldsymbol{\mathcal{Q}}_5\| \leq c_2\omega_2\|\boldsymbol{\mathcal{Q}}_R\| \end{cases} \tag{17}$$

Remark 1. Since $\boldsymbol{\mathcal{A}}_1$ is Hurwitz matrix in (16), there exists a positive definite matrix $\boldsymbol{\mathcal{P}}$ satisfying $\boldsymbol{\mathcal{A}}_1^T\boldsymbol{\mathcal{P}} + \boldsymbol{\mathcal{P}}\boldsymbol{\mathcal{A}}_1 = -\boldsymbol{I}_9$. Select observer bandwidth $\omega_1 > 2c_1\|\boldsymbol{\mathcal{P}}\boldsymbol{\mathcal{L}}_2\|$ for translational subsystem and Substituting $\boldsymbol{\mathcal{A}}_1$ into the above equation, it comes $\boldsymbol{\mathcal{P}} = \begin{bmatrix} \boldsymbol{I}_3 & -0.5\boldsymbol{I}_3 & -\boldsymbol{I}_3 \\ -0.5\boldsymbol{I}_3 & \boldsymbol{0} & -0.5\boldsymbol{I}_3 \\ -\boldsymbol{I}_3 & -0.5\boldsymbol{I}_3 & 4\boldsymbol{I}_3 \end{bmatrix}$. Then choose the following Lyapunov candidate function as:

$$V(\boldsymbol{\mathcal{Q}}_T) = \boldsymbol{\mathcal{Q}}_T^T\boldsymbol{\mathcal{P}}\boldsymbol{\mathcal{Q}}_T \tag{18}$$

Substituting (16) and (17) into the time derivative of $V(\mathcal{Q}_T)$, it has

$$\begin{aligned}\dot{V}(\mathcal{Q}_T) &= \dot{\mathcal{Q}}_T^T\mathcal{P}\mathcal{Q}_T + \mathcal{Q}_T^T\mathcal{P}\dot{\mathcal{Q}}_T \\ &= \omega_1\mathcal{Q}_T^T\mathcal{A}_1^T\mathcal{P}\mathcal{Q}_T + \left(\frac{\mathcal{L}_2\left(f_2(X_2)-f_2\left(\hat{X}_2\right)\right)}{\omega_1}\right)^T\mathcal{P}\mathcal{Q}_T + \left(\frac{\mathcal{L}_3\boldsymbol{h}_3}{\omega_1^2}\right)^T\mathcal{P}\mathcal{Q}_T + \omega_1\mathcal{Q}_T^T\mathcal{P}\mathcal{A}_1\mathcal{Q}_T \\ &\quad + \mathcal{Q}_T^T\mathcal{P}\frac{\mathcal{L}_2\left(f_2(X_2)-f_2\left(\hat{X}_2\right)\right)}{\omega_1} + \mathcal{Q}_T^T\mathcal{P}\mathcal{L}_3\frac{\mathcal{L}_3\boldsymbol{h}_3}{\omega_1^2} = \omega_1\mathcal{Q}_T^T\left(\mathcal{A}_1^T\mathcal{P}+\mathcal{P}\mathcal{A}_1\right)\mathcal{Q}_T \\ &\quad + \left(\frac{\mathcal{L}_2\left(f_2(X_2)-f_2\left(\hat{X}_2\right)\right)}{\omega_1}\right)^T\mathcal{P}\mathcal{Q}_T + \left(\frac{\mathcal{L}_3\boldsymbol{h}_3}{\omega_1^2}\right)^T\mathcal{P}\mathcal{Q}_T + \omega_1\mathcal{Q}_T^T\mathcal{P}\mathcal{A}_1\mathcal{Q}_T \\ &\quad + \mathcal{Q}_T^T\mathcal{P}\frac{\mathcal{L}_2\left(f_2(X_2)-f_2\left(\hat{X}_2\right)\right)}{\omega_1} + \mathcal{Q}_T^T\mathcal{P}\mathcal{L}_3\frac{\mathcal{L}_3\boldsymbol{h}_3}{\omega_1^2} \end{aligned} \tag{19}$$

According to Remark 1, $\mathcal{P}$ is a symmetric positive definite matrix, it comes from (19) that

$$\left(\frac{\mathcal{L}_2\left(f_2(X_2)-f_2\left(\hat{X}_2\right)\right)}{\omega_1}\right)^T\mathcal{P}\mathcal{Q}_T = \mathcal{Q}_T^T\mathcal{P}\frac{\mathcal{L}_2\left(f_2(X_2)-f_2\left(\hat{X}_2\right)\right)}{\omega_1}\left(\frac{\mathcal{L}_3\boldsymbol{h}_3}{\omega_1^2}\right)^T\mathcal{P}\mathcal{Q}_T = \mathcal{Q}_T^T\mathcal{P}\frac{\mathcal{L}_3\boldsymbol{h}_3}{\omega_1^2} \tag{20}$$

Substituting (20) into (19), we have

$$\begin{aligned}\dot{V}(\mathcal{Q}_T) &= \omega_1\mathcal{Q}_T^T(-\boldsymbol{I}_9)\mathcal{Q}_T + 2\mathcal{Q}_T^T\mathcal{P}\frac{\mathcal{L}_2 f_2(\mathbf{X}_2)-f_2(\hat{\boldsymbol{X}}_2)}{\omega_1} + 2\mathcal{Q}_T^T\mathcal{P}\frac{\mathcal{L}_3\boldsymbol{h}_3}{\omega_1^2} \\ &\le -\omega_1||\mathcal{Q}_T||^2 + 2\mathcal{Q}_T^T\mathcal{P}\frac{\mathcal{L}_2(c_1\omega_1||\mathcal{Q}_T||)}{\omega_1} + 2\mathcal{Q}_T^T\mathcal{P}\frac{\mathcal{L}_3\cdot\varepsilon_1}{\omega_1^2} \\ &\le -\omega_1\|\mathcal{Q}_T\|^2 + \frac{2c_1\omega_1\|\mathcal{Q}_T\|\cdot\|\mathcal{P}\mathcal{L}_2\|\cdot\|\mathcal{Q}_T\|}{\omega_1} + \frac{2\varepsilon_1\|\mathcal{Q}_T\|\cdot\|\mathcal{P}\mathcal{L}_3\|}{\omega_1^2} \\ &= -(\omega_1-2c_1\|\mathcal{P}\mathcal{L}_2\|)\|\mathcal{Q}_T\|^2 - \left(\frac{-2\varepsilon_1\|\mathcal{P}\mathcal{L}_3\|}{\omega_1^2}\right)\|\mathcal{Q}_T\| \\ &= -\|\mathcal{Q}_T\|\left((\omega_1-2c_1\|\mathcal{P}\mathcal{L}_2\|)\|\mathcal{Q}_T\| - \frac{2\varepsilon_1\|\mathcal{P}\mathcal{L}_3\|}{\omega_1^2}\right) \end{aligned} \tag{21}$$

Therefore, the designed MIMO-ESO is stable, and the estimation error will be bounded with $\|\mathcal{Q}_T\| \le \frac{2\varepsilon_1\|\mathcal{P}\mathcal{L}_3\|}{(\omega_1-2c_1\|\mathcal{P}\mathcal{L}_2\|)\omega_1^2}$ after a finite time, that is, the estimated velocity variable $\hat{\boldsymbol{X}}_2$ can track the real velocity precisely. According to Remark 1, $\omega_1 > 2c_1\|\mathcal{P}\mathcal{L}_2\|$ means a sufficiently large ω_1 can reduce the upper bound of the estimation error.

Remark 2. The stability proof for rotational subsystems is the same as for translational subsystem from (18) to (19). The observer bandwidth in rotational subsystem is selected as $\omega_2 > 2c_2\|\mathcal{P}\mathcal{L}_2\|$, the derivative of the Lyapunov function $\dot{V}(\mathcal{Q}_R) \le -\|\mathcal{Q}_R\|((\omega_2-2c_2\|\mathcal{P}\mathcal{L}_2\|)\cdot\|\mathcal{Q}_R\| - 2\varepsilon_2\|\mathcal{P}\mathcal{L}_3\|\cdot\omega_2^{-2})$**,** therefore, the upper bound for estimation error in rotational subsystem is $\|\mathcal{Q}_R\| \le \frac{2\varepsilon_2\|\mathcal{P}\mathcal{L}_3\|}{(\omega_2-2c_2\|\mathcal{P}\mathcal{L}_2\|)\omega_2^2}$ and inversely proportional to the value of the bandwidth.

Remark 3. The larger observer bandwidth ω_1 and ω_2 can reduce the estimation error but may lead to the high-frequency oscillation due to the high-gain integration, which will reduce

the robustness of the MIMO-ESO and the whole control system. Therefore, designers should consider an appropriate compromise/ trade-off between the estimation quality and the system robustness.

4. Controller design and analysis

To accomplish this position and attitude control system for, a decoupling algorithm and robust UDSMC method is presented in this section. Fig. 2 shows the quadrotor control framework, where IMU is internal measurement unit, providing basic motion and rotation information of the quadrotor aircraft, UDSMC is U-model based double sliding controller module.

4.1. UDSMC

4.1.1. U-control - U-model based control

U-model, a solely interested input and output mapping with time varying parameters absorbing the other dynamic variables and coefficients, is a class of derived control-orientated structure, which could be converted from any existing data driven and principal models [32]. By inverting the U-model, the control systems can be designed independently from model information. The U-control is shortened from U-model based control. In the past decade, U-control as a new control method has been well studied. Interesting readers can find the representative publications from the reference list.

U-model based control (U-control) can separate the controlled plant inversion and baseline controller design in double feedback loops. Fig. 3 shows the Continues-time (CT) U-control

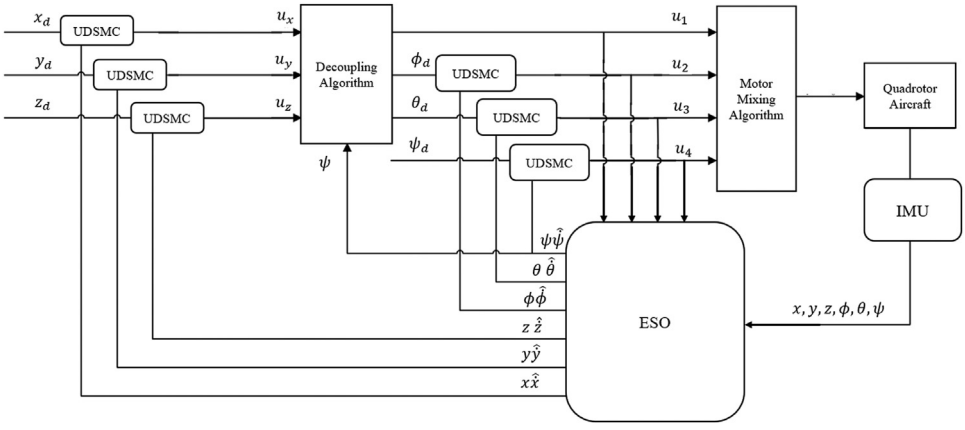

Fig. 2. The quadrotor control framework.

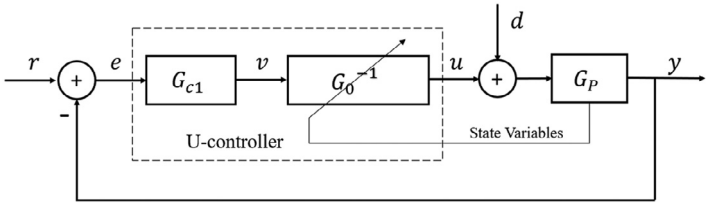

Fig. 3. U-control design framework.

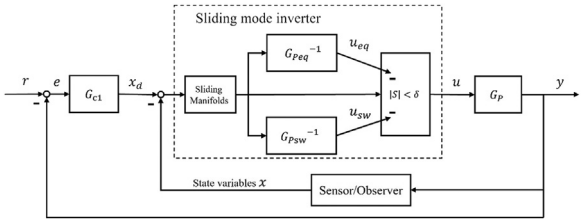

Fig. 4. UDSMC system design framework.

system framework [32]. The inner loop in U-control is plant's dynamic inversion design to cancel system nonlinearities and dynamics, that is, for a model-matched U-control framework, the product of the dynamic inverter and controlled plant should be converted into an identity matrix or a unit constant. Therefore, this U-control can become universal phase delay-free, fast-response and convenient but highly sensitive to the modelling errors and disturbances, which requires robust dynamic inversion algorithm [33–35]. The output of U-control system is specified with a second order linear dynamic (of course, user can assign the other types of controllers) below

$$y = \frac{G_{c1}G_0^{-1}G_P}{1 + G_{c1}G_0^{-1}G_P}r + \frac{G_P}{1 + G_{c1}G_0^{-1}G_P}d \tag{22}$$

where G_{c1} denotes a linear invariant controller, G_P denotes the controlled plant and G_0^{-1} denotes its regular inverter. r is the reference tracking signal. Model G_P equals G_0 achieves when system is free of system external disturbance and modelling errors, remarkably, the output of U-control system (17) can be simplified when $G_P = G_0$:

$$y = \frac{G_{c1}}{1 + G_{c1}}r = Gr \tag{23}$$

Concretely, G is the gain of the whole closed-loop control system, which can be designed and adjusted by typically different damping ratio ζ and natural frequency ω_n of G_{c1}.

Remark 4. The implementation of inversion requires the controlled plant be Bounded Input and Bounded Output (BIBO) stable and no unstable zero dynamic [44]. When the highest-order derivatives of system input $u^{(m)}$ is solved, the other u relative derivatives can be obtained by do integral operation of $u^{(m)}$.

4.1.2. UDSMC

Section 4.1.1 gives the basic concept of U-control system. The conventional U-inverter is sensitive to the accuracy of system modelling, which will therefore result in suboptimal control performance in practical control applications. Zhu et al. first used DSMC method to derive a robust dynamic inverter G_0^{-1} in DUSMC [29] of the controlled plant G_P. For a model-mismatched U-control framework, the feedback loop gain containing the dynamic inverter (sliding mode inverter) and controlled plant should be converted into an identity matrix or a unit constant [29]. The UDSMC design framework is shown in Fig. 4, where x_d is the desired state variables, ${G_{Psw}}^{-1}$ and ${G_{Peq}}^{-1}$are dynamic inverters when sliding manifold S_g stays outside and inside the sliding boundary δ, respectively; u_{sw} and u_{eq} are switching and equivalent controller, respectively. The block in Fig. 4 containing $|s| < \delta$ is a selection

switch module, which means that when $|s| < \delta$, u_{eq} will be activated, otherwise u_{sw} will be activated. The two-step independent design procedure of UDSMC is described as follows:

1) Using DSMC to design the inverter in the inner loop (cancellation of both nonlinearity and dynamics of the plant so that the external loop controller design has no request of plant model information, that is model-free controller design in the external loop)
The double sliding mode inverter (DSMI) in inner loop aims to achieve $G_0^{-1}G_P = 1$. The DSMI design procedure is described as follows
   i. Design global sliding manifold S_g with the boundary δ in the SM interval to specify the controlled system with the desired control performance specification:

$$S_g = S + \delta_1, \ \ 0 \le |\delta_1| \le \delta \tag{24}$$

   where $S = ce + \dot{e}$ is the classical sliding manifold function, c is the sliding coefficient.
   ii. Design the switching controller u_{sw} to drive the system states to the sliding manifold (with the boundary) and ensure that the system state slides on the manifold. Let $\dot{S}_g = f_g + f_u u_{sw}$, where f_g represents all the neglected bounded terms in the classical SMC design, then it comes

$$u_{sw} = -k_g sgn(S_g) \tag{25}$$

   iii. where $k_g \in \mathbb{R}^+$ is a positive gain coefficient and $sgn(*)$ is the sign function.
   iv. Design a local sliding manifold S_l with the equivalent controller u_{eq}. With the satisfaction of the classical Hurwitz stable, $S_l = S$. Let $\dot{S}_l = f_l + f_u u_{eq}$, where f_l represents all the neglected bounded terms in the classical SMC design. Consider the matching condition of $f_l = k_2$ be satisfied, where k_2 is a bounded tangent factor associated with S, then it comes

$$u_{eq} = -k_l S \tag{26}$$

   v. Finally, the DSM controller is designed as $u = u_{eq} + u_{sw} = -(k_g sgn(S_g) + k_l S)$

   Remark 5. It should be mentioned that the model inversion should exist and satisfy the Lipschitz continuity with globally uniformly [29]:

$$\|G(x_1) - G(x_2)\| \le \gamma_1 G \|x_1 - x_2\|, \ \ \forall x_1, x_2 \in \mathbb{R}^n$$

$$\|G^{-1}(x_1) - G^{-1}(x_2)\| \le \gamma_2 G^{-1} \|x_1 - x_2\|, \ \ \forall x_1, x_2 \in \mathbb{R}^n$$

2) Designing the invariant controller in the external loop (specify the control system performance)
Design a linear invariant controller G_{c1} with customer-defined damping ratio ζ and undamped natural frequency ω_n, that is, $G_{c1} = \frac{G}{1-G}$ and $G = \frac{\omega_n^2}{s^2 + 2\zeta\omega_n s + \omega_n^2}$.

4.2. Decoupling algorithm

Inspired by [36], assume system (8) is fully actuated and convert it into

$$\begin{cases} \ddot{x} = u_x - \frac{1}{m_s} K_1 \dot{x} \\ \ddot{y} = u_y - \frac{1}{m_s} K_2 \dot{y} \\ \ddot{z} = u_z - g - \frac{1}{m_s} K_3 \dot{z} \end{cases} \tag{27}$$

where u_x, u_y and u_z are assumed position controllers shown as:

$$\begin{cases} u_x = \frac{u_1}{m_s}(cos\ \psi \sin\theta cos\ \phi + \ \sin\phi \sin\psi\ ) \\ u_y = \frac{u_1}{m_s}(\sin\psi \sin\theta cos\ \phi - cos\ \psi \sin\phi) \\ u_z = \frac{u_1}{m_s}(cos\ \theta cos\ \phi) \end{cases} \tag{28}$$

By squaring both sides of the above equations, it comes:

$$\frac{u_1}{m_s} = \sqrt{u_x^2 + u_y^2 + u_z^2} = \frac{u_z}{cos\ \theta cos\ \phi} \tag{29}$$

Therefore, the desired roll and pitch angles (ϕ_d, θ_d) can be calculated by:

$$\phi_d = \arcsin\left(m_s \frac{u_x sin\psi - u_y cos\psi}{u_1}\right) \tag{30}$$

$$\theta_d = \arctan\left(\frac{u_x cos\psi + u_y sin\psi}{u_z}\right) \tag{31}$$

Remark 6. It should be noticed that the roll, pitch and yaw angles (ϕ, θ, ψ) are bounded and meet the satisfaction of: $\phi, \theta \in (-\pi/2, \pi/2)$ and $\psi \in (-\pi, \pi)$, which are necessarily considered avoiding the singularity problems in the aerodynamic and controller design [30].

Assuming the body of quadrotor is rigid, the position controllers for x and y are designed by using UDSMC method. According to system (23), the sliding manifolds and their derivatives are defined as

$$\boldsymbol{S}_P = \boldsymbol{C}_P \boldsymbol{e}_P + \dot{\hat{\boldsymbol{e}}}_P,\ \boldsymbol{S}_{P1} = \boldsymbol{S}_P + \boldsymbol{\delta}_P, \boldsymbol{S}_{P2} = \boldsymbol{S}_P, \dot{\boldsymbol{S}}_{P1} = \boldsymbol{f}_P + \boldsymbol{U}_{Psw}, \dot{\boldsymbol{S}}_{P2} = \boldsymbol{K}_P + \boldsymbol{U}_{Peq} \tag{32}$$

where $\boldsymbol{S}_P = [S_x, S_y, S_z]^T$, $\boldsymbol{S}_{P1} = [S_{x1}, S_{y1}, S_{z1}]^T$, $\boldsymbol{C}_P$ is designed positive definite diagonal matric, $\boldsymbol{e}_P = [e_x, e_y, e_z]^T = [x - x_d, y - y_d, z - z_d]^T$, $\boldsymbol{\delta}_P = [\delta_x, \delta_y, \delta_z]^T$, $\boldsymbol{f}_P = [f_x, f_y, f_z]^T$ with $f_x = c_x\dot{\hat{e}}_x - \frac{1}{m_s}K_1\dot{\hat{x}}$, $f_y = c_y\dot{\hat{e}}_y - \frac{1}{m_s}K_2\dot{\hat{y}}$ and $f_z = c_z\dot{\hat{e}}_z - g - \frac{1}{m_s}K_3\dot{\hat{z}}$; $\boldsymbol{K}_P$ is bounded unknown tangent matrices of $\boldsymbol{S}_P$. The corresponding position controllers are designed as:

$$\boldsymbol{U}_P = -\boldsymbol{K}_{P1}\mathbf{sgn}(\boldsymbol{S}_{P1}) - \boldsymbol{K}_{P2}\boldsymbol{S}_{P2} \tag{33}$$

where $\boldsymbol{K}_{P1}$ and $\boldsymbol{K}_{P2}$ are designed positive definite diagonal matrices, $\boldsymbol{U}_P = \boldsymbol{U}_{Psw} + \boldsymbol{U}_{Peq}$, $\mathbf{sgn}(\boldsymbol{S}_{P1}) = [\mathrm{sgn}(S_{x1}), \mathrm{sgn}(S_{y1}), \mathrm{sgn}(S_{z1})]^T$.

Assuming a Lyapunov function $\boldsymbol{V}_P = \frac{1}{2}\boldsymbol{S}_{P1}^T\boldsymbol{S}_{P1} + \frac{1}{2}\boldsymbol{S}_{P2}^T\boldsymbol{S}_{P2}$, its corresponding derivative is:

$$\begin{aligned} \dot{\boldsymbol{V}}_P &= \frac{1}{2}\dot{\boldsymbol{S}}_{P1}^T\boldsymbol{S}_{P1} + \frac{1}{2}\dot{\boldsymbol{S}}_{P2}^T\boldsymbol{S}_{P2} + \frac{1}{2}\boldsymbol{S}_{P1}^T\dot{\boldsymbol{S}}_{P1} + \frac{1}{2}\boldsymbol{S}_{P2}^T\dot{\boldsymbol{S}}_{P2} \le \boldsymbol{S}_{P1}^T\dot{\boldsymbol{S}}_{P1} + \boldsymbol{S}_{P2}^T\dot{\boldsymbol{S}}_{P2} \\ &= \boldsymbol{S}_{P1}^T(\boldsymbol{f}_P - \boldsymbol{K}_{P1}\mathbf{sgn}(\boldsymbol{S}_{P1})) + \boldsymbol{S}_{P2}^T(\boldsymbol{K}_P - \boldsymbol{K}_{P2}\boldsymbol{S}_{P2}) \\ &\le -\|\boldsymbol{S}_{P1}\|(\boldsymbol{K}_{P1} - \boldsymbol{f}_P) - \|\boldsymbol{S}_{P2}\|(\boldsymbol{K}_{P2} - \boldsymbol{K}_P) \end{aligned} \tag{34}$$

To satisfy $\dot{\boldsymbol{V}}_P < 0$ for horizontal position control stability, it comes $\boldsymbol{K}_{P1} - \boldsymbol{f}_P > 0$, $\boldsymbol{K}_{P2} - \boldsymbol{K}_P > 0$, therefore

$$\boldsymbol{K}_{P1} > \|\boldsymbol{f}_P\| \text{ and } \boldsymbol{K}_{P2} > \|\boldsymbol{K}_P\| \tag{35}$$

Remark 7. This study divides the control system into two main subsystems: fully actuated subsystem composed of z and ψ and underactuated subsystem composed of x, θ and y, ϕ. According to Fig. 1, for a given reference positions x_d and y_d, this study first converts system (14) into a fully actuated control system, and its position controllers are designed respectively by using UDSMC method. Then the desired angles reference for positions control are calculated through the decoupling system accordingly. Next, the design steps of the subsequent fully actuated and underactuated controller will be introduced in detail.

4.3. Uncoupled/fully actuated subsystem controller

Fully actuated subsystem controller is designed by UDSMC method to ensure the altitude variables z and yaw angle ψ can converge to their desired values z_d and ψ_d. Additionally, assuming that the structure of quadrotor is rigid and symmetrical, therefore, the sliding manifolds are designed as

$$\boldsymbol{S}_F = \boldsymbol{C}_F\boldsymbol{e}_F + \dot{\hat{e}}_F, \boldsymbol{S}_{F1} = \boldsymbol{S}_F + \boldsymbol{\delta}_F, \boldsymbol{S}_{F2} = \boldsymbol{S}_F, \dot{\boldsymbol{S}}_{F1} = \boldsymbol{f}_F + \boldsymbol{f}_{FU}\boldsymbol{U}_{Fsw}, \dot{\boldsymbol{S}}_{F2} = \boldsymbol{K}_F + \boldsymbol{f}_{FU}\boldsymbol{U}_{Feq} \quad (36)$$

where $\boldsymbol{S}_F = [S_1, S_4]^T$ are sliding manifolds for fully actuated subsystem, $\boldsymbol{S}_{F1} = [S_{g1}, S_{g4}]^T$, $\boldsymbol{C}_F = diag(c_z, c_\psi)$ is designed positive definite diagonal matric, $\boldsymbol{e}_F = [e_z, e_\psi]^T = [z - z_d, \psi - \psi_d]^T$, $\boldsymbol{\delta}_F = [\delta_z, \delta_\psi]^T$, $\boldsymbol{f}_F = [f_{g1}, f_{g4}]^T$ with $f_{g1} = c_z\dot{\hat{e}}_z = g - \frac{1}{m_s}k_3\dot{\hat{z}} - \ddot{\hat{z}}_d$ and $f_{g4} = c_\psi\dot{\hat{e}}_\psi + pq\frac{I_x - I_y}{I_z} - \frac{k_6}{I_z}r - \ddot{\psi}_d$; $\boldsymbol{f}_{FU} = \text{diag}(f_{u1}, f_{u4})$ with $f_{u1} = 1$ and $f_{u4} = \frac{C}{I_z}$; $\boldsymbol{K}_F$ is bounded unknown tangent matrices of $\boldsymbol{S}_F$. $\boldsymbol{U}_{Fsw} = [u_{1sw}, u_{4sw}]^T$ is the switching controller and $\boldsymbol{U}_{Feq} = [u_{1eq}, u_{4eq}]^T$ is the equivalent controller. The corresponding controllers for this fully actuated subsystem are designed as:

$$\boldsymbol{U}_F = -\boldsymbol{K}_{F1}\mathbf{sgn}(\boldsymbol{S}_{F1}) - \boldsymbol{K}_{F2}\boldsymbol{S}_{F2} \quad (37)$$

where $\boldsymbol{K}_{F1}$ and $\boldsymbol{K}_{F2}$ are designed positive definite diagonal matrices, $\boldsymbol{U}_F = [u_1, u_4]^T = \boldsymbol{U}_{Fsw} + \boldsymbol{U}_{Feq}$, $\mathbf{sgn}(\boldsymbol{S}_{F1}) = [\text{sgn}(S_{g1}), \text{sgn}(S_{g4})]^T$.

Assuming a Lyapunov function $\boldsymbol{V}_F = \frac{1}{2}\boldsymbol{S}_{F1}^T\boldsymbol{S}_{F1} + \frac{1}{2}\boldsymbol{S}_{F2}^T\boldsymbol{S}_{F2}$, its corresponding derivative is:

$$\begin{aligned}\dot{\boldsymbol{V}}_F &= \frac{1}{2}\dot{\boldsymbol{S}}_{F1}^T\boldsymbol{S}_{F1} + \frac{1}{2}\dot{\boldsymbol{S}}_{F2}^T\boldsymbol{S}_{F2} + \frac{1}{2}\boldsymbol{S}_{F1}^T\dot{\boldsymbol{S}}_{F1} + \frac{1}{2}\boldsymbol{S}_{F2}^T\dot{\boldsymbol{S}}_{F2} \le \boldsymbol{S}_{F1}^T\dot{\boldsymbol{S}}_{F1} + \boldsymbol{S}_{F2}^T\dot{\boldsymbol{S}}_{F2} \\ &= \boldsymbol{S}_{F1}^T(\boldsymbol{f}_F - \boldsymbol{f}_{FU}(\boldsymbol{K}_{F1}\mathbf{sgn}(\boldsymbol{S}_{F1}))) + \boldsymbol{S}_{P2}^T(\boldsymbol{K}_F - \boldsymbol{f}_{FU}(\boldsymbol{K}_{F2}\boldsymbol{S}_{F2})) \\ &\le -\|\boldsymbol{S}_{F1}\|(\boldsymbol{f}_{FU}\boldsymbol{K}_{F1} - \boldsymbol{f}_F) - \|\boldsymbol{S}_{F2}\|(\boldsymbol{f}_{FU}\boldsymbol{K}_{F2} - \boldsymbol{K}_F)\end{aligned} \quad (38)$$

To satisfy $\dot{\boldsymbol{V}}_F < 0$ for altitude control and yaw angle control stability, it comes $\boldsymbol{f}_{FU}\boldsymbol{K}_{F1} - \boldsymbol{f}_F > 0$ and $\boldsymbol{f}_{FU}\boldsymbol{K}_{F2} - \boldsymbol{K}_F > 0$, therefore

$$\boldsymbol{K}_{F1} > \|\boldsymbol{f}_F\|\boldsymbol{f}_{FU}^{-1} \text{ and } \boldsymbol{K}_{P2} > \|\boldsymbol{K}_F\|\boldsymbol{f}_{FU}^{-1} \quad (39)$$

Remark 8. According to Eqs. (28) and (42), the relationship between u_z and u_1 is: $u_z = \frac{u_1 cos\ \theta cos\ \phi}{m_s}$. Therefore, the design of u_1 can be converted into the design of u_z.

4.4. Coupled/underactuated subsystem controller

Underactuated subsystem controller is also designed by UDSMC method to maintain the horizontal position variables $[x,\ y]$ and pitch and roll angles variables $[\phi, \theta]$ can converge to their desired values $[x_d,\ y_d]$ and $[\phi_d, \theta_d]$ with only two control inputs u_2 and u_3. Accordingly, the sliding manifolds are designed as

$$\begin{aligned}\boldsymbol{S}_{UN} &= \boldsymbol{C}_{UN1}\boldsymbol{e}_{UN1} + \boldsymbol{C}_{UN2}\dot{\hat{\boldsymbol{e}}}_{Un1} + \boldsymbol{C}_{UN3}\boldsymbol{e}_{UN2} + \boldsymbol{C}_{UN4}\dot{\hat{\boldsymbol{e}}}_{Un2}\boldsymbol{S}_{UN1} \\ &= \boldsymbol{S}_{UN} + \boldsymbol{\delta}_{UN},\ \boldsymbol{S}_{UN2} = \boldsymbol{S}_{UN}\dot{\boldsymbol{S}}_{UN1} = \boldsymbol{f}_{UN} + \boldsymbol{f}_{UNU}\boldsymbol{U}_{UNsw} \\ \dot{\boldsymbol{S}}_{UN2} &= \boldsymbol{K}_{UN} + \boldsymbol{f}_{UNU}\boldsymbol{U}_{UNeq}\end{aligned} \quad (40)$$

where $\boldsymbol{S}_{UN} = [S_2, S_3]^T$ are sliding manifolds for fully actuated subsystem, $\boldsymbol{S}_{UN1} = [S_{g2}, S_{g3}]^T$; $\boldsymbol{C}_{UN1} = \text{diag}(c_1, c_5)$, $\boldsymbol{C}_{UN2} = \text{diag}(c_2, c_6)$, $\boldsymbol{C}_{UN3} = \text{diag}(c_3, c_7)$, $\boldsymbol{C}_{UN4} =$

diag(c_4, c_8) are designed positive definite diagonal matrices, $\boldsymbol{e}_{UN1} = [e_x, e_y]^T = [x - x_d, y - y_d]^T$, $\boldsymbol{e}_{UN2} = [e_\theta, e_\phi]^T = [\theta - \theta_d, \phi - \phi_d]^T$ $\boldsymbol{\delta}_{UN} = [\delta_2, \delta_3]^T$, $\boldsymbol{f}_{UN} = [f_{g2}, f_{g3}]^T$ with $f_{g2} = c_1\ddot{e}_y + c_2\dot{\hat{e}}_y + c_3(\hat{q}\hat{r}\frac{I_y - I_z}{I_x} + \frac{J_r}{I_x}\hat{q}\Omega_r - \frac{k_4 l}{I_x}\hat{p}) - \ddot{\phi}_d + c_4\dot{\hat{e}}_\phi$ and $f_{g3} = c_5\ddot{\hat{e}}_x + c_6\dot{\hat{e}}_x + c_7(\hat{p}\hat{r}\frac{I_z - I_x}{I_y} - \frac{J_r}{I_y}\hat{p}\Omega_r - \frac{k_5 l}{I_y}\hat{q}) - \ddot{\theta}_d + c_8\dot{\hat{e}}_\theta$; $\boldsymbol{f}_{UNU} = \text{diag}(f_{u2}, f_{u3})$ with $f_{u2} = \frac{c_3 l}{I_x}$ and $f_{u3} = \frac{c_7 l}{I_y}$; $\boldsymbol{K}_{UN}$ is bounded unknown tangent matrices of $\boldsymbol{S}_{UN}$. $\boldsymbol{U}_{UNsw} = [u_{2sw}, u_{3sw}]^T$ is the switching controller and $\boldsymbol{U}_{UNeq} = [u_{2eq}, u_{3eq}]^T$ is the equivalent controller. The corresponding controllers for this fully actuated subsystem are designed as:

$$\boldsymbol{U}_{UN} = -\boldsymbol{K}_{UN1}\mathbf{sgn}(\boldsymbol{S}_{UN1}) - \boldsymbol{K}_{UN2}\boldsymbol{S}_{UN2} \tag{41}$$

where $\boldsymbol{K}_{UN1}$ and $\boldsymbol{K}_{UN2}$ are designed positive definite diagonal matrices, $\boldsymbol{U}_{UN} = [u_2, u_3]^T = \boldsymbol{U}_{UNsw} + \boldsymbol{U}_{UNeq}$, $\mathbf{sgn}(\boldsymbol{S}_{UN1}) = [\text{sgn}(S_{g2}), \text{sgn}(S_{g3})]^T$. Assuming a Lyapunov function $\boldsymbol{V}_{UN} = [V_2, V_3]^T = \frac{1}{2}\boldsymbol{S}_{UN1}^T\boldsymbol{S}_{UN1} + \frac{1}{2}\boldsymbol{S}_{UN2}^T\boldsymbol{S}_{UN2}$, its corresponding derivative is:

$$\begin{aligned}\dot{\boldsymbol{V}}_{UN} &= \frac{1}{2}\dot{\boldsymbol{S}}_{UN1}^T\boldsymbol{S}_{UN1} + \frac{1}{2}\dot{\boldsymbol{S}}_{UN2}^T\boldsymbol{S}_{UN2} + \frac{1}{2}\boldsymbol{S}_{UN1}^T\dot{\boldsymbol{S}}_{UN1} + \frac{1}{2}\boldsymbol{S}_{UN2}^T\dot{\boldsymbol{S}}_{UN2} \le \boldsymbol{S}_{UN1}^T\dot{\boldsymbol{S}}_{UN1} + \boldsymbol{S}_{UN2}^T\dot{\boldsymbol{S}}_{UN2} \\ &= \boldsymbol{S}_{UN1}^T(\boldsymbol{f}_{UN} - \boldsymbol{f}_{UNU}(\boldsymbol{K}_{UN1}\mathbf{sgn}(\boldsymbol{S}_{UN1}))) + \boldsymbol{S}_{UN2}^T(\boldsymbol{K}_{UN} - \boldsymbol{f}_{UNU}(\boldsymbol{K}_{UN2}\boldsymbol{S}_{UN2})) \\ &\le -\|\boldsymbol{S}_{UN1}\|(\boldsymbol{f}_{UNU}\boldsymbol{K}_{UN1} - \boldsymbol{f}_{UN}) - \|\boldsymbol{S}_{UN2}\|(\boldsymbol{f}_{UNU}\boldsymbol{K}_{UN2} - \boldsymbol{K}_{UN})\end{aligned} \tag{42}$$

To satisfy $\dot{V}_2 < 0$ for x position and roll angle control stability and $\dot{V}_3 < 0$ for y position and pitch angle control stability, it comes $\boldsymbol{f}_{UNU}\boldsymbol{K}_{UN1} - \boldsymbol{f}_{UN} > 0$ and $\boldsymbol{f}_{UNU}\boldsymbol{K}_{UN2} - \boldsymbol{K}_{UN} > 0$, therefore

$$\boldsymbol{K}_{UN1} > \|\boldsymbol{f}_{UN}\|\boldsymbol{f}_{UNU}^{-1} \text{ and } \boldsymbol{K}_{UN2} > \|\boldsymbol{K}_{UN}\|\boldsymbol{f}_{UNU}^{-1} \tag{43}$$

4.5. The sliding manifolds coefficients

Let the sliding manifold S_2 and its derivative equal to zero:

$$\boldsymbol{S}_{UN} = \boldsymbol{C}_{UN1}\boldsymbol{e}_{UN1} + \boldsymbol{C}_{UN2}\dot{\hat{\boldsymbol{e}}}_{UN1} + \boldsymbol{C}_{UN3}\boldsymbol{e}_{UN2} + \boldsymbol{C}_{UN4}\dot{\hat{\boldsymbol{e}}}_{UN2} = 0 \tag{44}$$

$$\dot{\boldsymbol{S}}_{UN} = \boldsymbol{C}_{UN1}\dot{\hat{\boldsymbol{e}}}_{UN1} + \boldsymbol{C}_{UN2}\ddot{\hat{\boldsymbol{e}}}_{UN1} + \boldsymbol{C}_{UN3}\dot{\hat{\boldsymbol{e}}}_{UN2} + \boldsymbol{C}_{UN4}\ddot{\hat{\boldsymbol{e}}}_{UN2} = 0 \tag{45}$$

From (45), it has

$$\ddot{\hat{\boldsymbol{e}}}_{UN2} = -\boldsymbol{C}_{UN4}^{-1}\left(\boldsymbol{C}_{UN1}\dot{\hat{\boldsymbol{e}}}_{UN1} + \boldsymbol{C}_{UN2}\ddot{\hat{\boldsymbol{e}}}_{UN1} + \boldsymbol{C}_{UN3}\dot{\hat{\boldsymbol{e}}}_{UN2}\right) \tag{46}$$

From (44), it comes

$$\dot{\hat{\boldsymbol{e}}}_{UN1} = -\boldsymbol{C}_{UN2}^{-1}\left(\boldsymbol{C}_{UN1}\boldsymbol{e}_{UN1} + \boldsymbol{C}_{UN3}\boldsymbol{e}_{UN2} + \boldsymbol{C}_{UN4}\dot{\hat{\boldsymbol{e}}}_{UN2}\right) \tag{47}$$

Substituting (47) into (46), it comes,

$$\begin{aligned}\ddot{\hat{\boldsymbol{e}}}_{UN2} &= -\boldsymbol{C}_{UN4}^{-1}\Big(\boldsymbol{C}_{UN1}\Big(-\boldsymbol{C}_{UN2}^{-1}\Big(\boldsymbol{C}_{UN1}\boldsymbol{e}_{UN1}+\boldsymbol{C}_{UN3}\boldsymbol{e}_{UN2}+\boldsymbol{C}_{UN4}\dot{\hat{\boldsymbol{e}}}_{UN2}\Big)\Big)+\boldsymbol{C}_{UN2}\ddot{\hat{\boldsymbol{e}}}_{UN1}+\boldsymbol{C}_{UN3}\dot{\hat{\boldsymbol{e}}}_{UN2}\Big)\\ &= \boldsymbol{C}_{UN4}^{-1}\boldsymbol{C}_{UN1}\boldsymbol{C}_{UN2}^{-1}\Big(\boldsymbol{C}_{UN1}\boldsymbol{e}_{UN1}+\boldsymbol{C}_{UN3}\boldsymbol{e}_{UN2}+\boldsymbol{C}_{UN4}\ddot{\hat{\boldsymbol{e}}}_{UN2}\Big)-\boldsymbol{C}_{UN4}^{-1}\boldsymbol{C}_{UN2}\ddot{\hat{\boldsymbol{e}}}_{UN1}-\boldsymbol{C}_{UN4}^{-1}\boldsymbol{C}_{UN3}\dot{\hat{\boldsymbol{e}}}_{UN2}\\ &= \boldsymbol{C}_{UN4}^{-1}\boldsymbol{C}_{UN1}\boldsymbol{C}_{UN2}^{-1}\boldsymbol{C}_{UN1}\boldsymbol{e}_{UN1}+\boldsymbol{C}_{UN4}^{-1}\boldsymbol{C}_{UN1}\boldsymbol{C}_{UN2}^{-1}\boldsymbol{C}_{UN3}\boldsymbol{e}_{UN2}\\ &\quad+\big(\boldsymbol{C}_{UN4}^{-1}\boldsymbol{C}_{UN1}\boldsymbol{C}_{UN2}^{-1}\boldsymbol{C}_{UN4}-\boldsymbol{C}_{UN4}^{-1}\boldsymbol{C}_{UN3}\big)\dot{\hat{\boldsymbol{e}}}_{UN2}-\boldsymbol{C}_{UN4}^{-1}\boldsymbol{C}_{UN2}\ddot{\hat{\boldsymbol{e}}}_{UN1}\end{aligned}\tag{48}$$

Let $\boldsymbol{Y}_1=\boldsymbol{e}_{UN2}$, $\boldsymbol{Y}_2=\dot{\boldsymbol{Y}}_1=\dot{\hat{\boldsymbol{e}}}_{UN2}$ and $\boldsymbol{Y}_3=\boldsymbol{e}_{UN1}$. The cascaded form is obtained as:

$$\begin{aligned}\dot{\boldsymbol{Y}}_1 &= \boldsymbol{Y}_2\\ \dot{\boldsymbol{Y}}_2 &= \boldsymbol{C}_{UN4}^{-1}\boldsymbol{C}_{UN1}\boldsymbol{C}_{UN2}^{-1}\boldsymbol{C}_{UN1}\boldsymbol{e}_{UN1}+\boldsymbol{C}_{UN4}^{-1}\boldsymbol{C}_{UN1}\boldsymbol{C}_{UN2}^{-1}\boldsymbol{C}_{UN3}\boldsymbol{e}_{UN2}+\big(\boldsymbol{C}_{UN4}^{-1}\boldsymbol{C}_{UN1}\boldsymbol{C}_{UN2}^{-1}\boldsymbol{C}_{UN4}-\boldsymbol{C}_{UN4}^{-1}\boldsymbol{C}_{UN3}\big)\boldsymbol{e}_{UN2}\\ &\quad-\boldsymbol{C}_{UN4}^{-1}\boldsymbol{C}_{UN2}\dot{\hat{\boldsymbol{e}}}_{UN2}\dot{\boldsymbol{Y}}_3=-\boldsymbol{C}_{UN2}^{-1}\boldsymbol{C}_{UN1}\boldsymbol{e}_{UN1}-\boldsymbol{C}_{UN2}^{-1}\boldsymbol{C}_{UN3}\boldsymbol{e}_{UN2}-\boldsymbol{C}_{UN2}^{-1}\boldsymbol{C}_{UN4}\boldsymbol{e}_{UN2}\end{aligned}\tag{49}$$

When the system state variables approach to their equilibrium points, that is, $\boldsymbol{e}_{UN2}\to 0$, $\dot{\hat{\boldsymbol{e}}}_{UN2}\to 0$, $\boldsymbol{e}_{UN1}\to 0$, thus, $\boldsymbol{Y}_1\to 0$, $\boldsymbol{Y}_2\to 0$, $\boldsymbol{Y}_3\to 0$. After the linearization operation around the equilibrium points, it comes

$$\ddot{\hat{\boldsymbol{e}}}_{UN1}=\boldsymbol{\mathcal{H}}\boldsymbol{e}_{UN2}+\boldsymbol{\mathcal{N}}\tag{50}$$

where $\boldsymbol{\mathcal{H}}=diag(u_1 cos\ \psi cos\ \phi/m_s,-u_1 cos\ \psi/m_s)$, $\boldsymbol{e}_{UN2}=[\theta-\theta_d,\phi-\phi_d]^T$, $\boldsymbol{\mathcal{N}}=[u_1\sin\phi\sin\psi/m_s-K_1\dot{\hat{x}}/m_s-\ddot{x}_d,u_1\sin\psi\sin\theta cos\ \phi/m_s-K_2\dot{\hat{y}}/m_s-\ddot{y}_d]^T$. Then substitute (50) into (49) and use $\boldsymbol{Y}_1$, $\boldsymbol{Y}_2$, $\boldsymbol{Y}_3$ to replace the related items, the new cascaded form is obtained after organization as:

$$\begin{aligned}\dot{\boldsymbol{Y}}_1 &= \boldsymbol{Y}_2\\ \dot{\boldsymbol{Y}}_2 &= \big(\boldsymbol{C}_{UN4}^{-1}\boldsymbol{C}_{UN1}\boldsymbol{C}_{UN2}^{-1}\boldsymbol{C}_{UN3}-\boldsymbol{C}_{UN4}^{-1}\boldsymbol{C}_{UN2}\boldsymbol{\mathcal{H}}\big)\boldsymbol{Y}_1+\big(\boldsymbol{C}_{UN4}^{-1}\boldsymbol{C}_{UN1}\boldsymbol{C}_{UN2}^{-1}\boldsymbol{C}_{UN4}-\boldsymbol{C}_{UN4}^{-1}\boldsymbol{C}_{UN3}\big)\boldsymbol{Y}_2\\ &\quad+\boldsymbol{C}_{UN4}^{-1}\boldsymbol{C}_{UN1}\boldsymbol{C}_{UN2}^{-1}\boldsymbol{C}_{UN1}\boldsymbol{Y}_3-\boldsymbol{C}_{UN4}^{-1}\boldsymbol{C}_{UN2}\boldsymbol{\mathcal{N}}\dot{\boldsymbol{Y}}_3\\ &= -\boldsymbol{C}_{UN2}^{-1}\boldsymbol{C}_{UN3}\boldsymbol{Y}_1-\boldsymbol{C}_{UN2}^{-1}\boldsymbol{C}_{UN4}\boldsymbol{Y}_2-\boldsymbol{C}_{UN2}^{-1}\boldsymbol{C}_{UN1}\boldsymbol{Y}_3\end{aligned}\tag{51}$$

Let $\boldsymbol{Y}=[\boldsymbol{Y}_1,\boldsymbol{Y}_2,\boldsymbol{Y}_3]^T$, its derivative matrix form is $\dot{\boldsymbol{Y}}=\boldsymbol{A}\boldsymbol{Y}$, where

$$\boldsymbol{A}=\begin{bmatrix}\boldsymbol{A}_{11}&\boldsymbol{A}_{12}&\boldsymbol{A}_{13}\\ \boldsymbol{A}_{21}&\boldsymbol{A}_{22}&\boldsymbol{A}_{23}\\ \boldsymbol{A}_{31}&\boldsymbol{A}_{32}&\boldsymbol{A}_{33}\end{bmatrix}\tag{52}$$

The matrix $\boldsymbol{A}$ is Hurwitz and the system states will be asymptotically approaching their equilibrium points [36]. Assuming $\boldsymbol{C}_{UN4}^{-1}\neq 0$ and $\boldsymbol{C}_{UN2}^{-1}\neq 0$, the parameters in (51) are obtained from (52):

$$\begin{aligned}&\boldsymbol{A}_{11}=\boldsymbol{A}_{13}=0,\boldsymbol{A}_{12}=\boldsymbol{I}_2\\ &\boldsymbol{A}_{21}=\boldsymbol{C}_{UN4}^{-1}\boldsymbol{C}_{UN1}\boldsymbol{C}_{UN2}^{-1}\boldsymbol{C}_{UN3}-\boldsymbol{C}_{UN4}^{-1}\boldsymbol{C}_{UN2}\boldsymbol{\mathcal{H}}\\ &\boldsymbol{A}_{22}=\boldsymbol{C}_{UN4}^{-1}\boldsymbol{C}_{UN1}\boldsymbol{C}_{UN2}^{-1}\boldsymbol{C}_{UN4}-\boldsymbol{C}_{UN4}^{-1}\boldsymbol{C}_{UN3}\\ &\boldsymbol{A}_{23}=\boldsymbol{C}_{UN4}^{-1}\boldsymbol{C}_{UN1}\boldsymbol{C}_{UN2}^{-1}\boldsymbol{C}_{UN1}\\ &\boldsymbol{A}_{31}=-\boldsymbol{C}_{UN2}^{-1}\boldsymbol{C}_{UN3},\ \boldsymbol{A}_{32}=-\boldsymbol{C}_{UN2}^{-1}\boldsymbol{C}_{UN4},\boldsymbol{A}_{33}=-\boldsymbol{C}_{UN2}^{-1}\boldsymbol{C}_{UN1}\end{aligned}\tag{53}$$

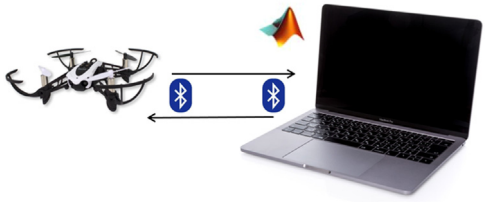

Fig. 5. Parrot Minidrone experimental platform.

Let $|\lambda \cdot \boldsymbol{I}_6 - \boldsymbol{A}| = 0$, that is,

$$\begin{vmatrix} \lambda \cdot \boldsymbol{I}_2 & -\boldsymbol{I}_2 & 0 \\ \boldsymbol{A}_{21} & \lambda \cdot \boldsymbol{I}_2 - A_{22} & \boldsymbol{A}_{23} \\ \boldsymbol{A}_{31} & \boldsymbol{A}_{32} & \lambda \cdot \boldsymbol{I}_2 - \boldsymbol{A}_{33} \end{vmatrix} = 0 \tag{54}$$

Determinant (54) can be calculated as:

$$(\lambda \cdot \boldsymbol{I}_2)^3 - (\boldsymbol{A}_{22} + \boldsymbol{A}_{33})(\lambda \cdot \boldsymbol{I}_2)^2 + (\boldsymbol{A}_{33}\boldsymbol{A}_{22} - \boldsymbol{A}_{21} - \boldsymbol{A}_{32}\boldsymbol{A}_{23})(\lambda \cdot \boldsymbol{I}_2) + (\boldsymbol{A}_{33}\boldsymbol{A}_{21} - \boldsymbol{A}_{31}\boldsymbol{A}_{23}) = 0 \tag{55}$$

Let the characteristic equation be $(\lambda \cdot \boldsymbol{I}_2 + 2\boldsymbol{I}_2)^3 = 0$, after the comparison this equation with (55), it has:

$$\begin{cases} -(\boldsymbol{A}_{22} + \boldsymbol{A}_{33}) = 6\boldsymbol{I}_2 \\ \boldsymbol{A}_{33}\boldsymbol{A}_{22} - \boldsymbol{A}_{21} - \boldsymbol{A}_{32}\boldsymbol{A}_{23} = 12\boldsymbol{I}_2 \\ \boldsymbol{A}_{33}\boldsymbol{A}_{21} - \boldsymbol{A}_{31}\boldsymbol{A}_{23} = 8\boldsymbol{I}_2 \end{cases} \tag{56}$$

After organization, Let $c_4 = c_8 = 1$, then the other coefficients are: $c_1 = \frac{8m_s}{u_1 cos\ \phi cos\ \psi}$, $c_2 = \frac{12m_s}{u_1 cos\ \phi cos\ \psi}$, $c_3 = 6$, $c_5 = -\frac{8m_s}{cos\ \psi u_1}$, $c_6 = -\frac{12m_s}{cos\ \psi u_1}$, $c_7 = 6$.

5. Experimental studies

The proposed ESO UDSMC based quadrotor control system has been tested by the Parrot Mambo Minidrone position tracking experiment. In order to evaluate the real-time position and attitude tracking performance of quadrotor under UDSMC method, its experiment results will be compared with the PID controller and sliding mode controller. The PID controller is the original built-in controller of the Parrot Minidrone and has been adjusted by the manufacturer for optimum performance.

5.1. Experiment setup

The Parrot Mambo Minidrone, which is shown in Fig. 5, is equipped with 6-DOF inertial measurement unit (3-axis accelerometer and 3-axis gyroscope), an ultrasound sensor and pressure sensors that can detect quadrotor's altitude, a pressure sensor, a 60FPS camera with a resolution of 120×160 pixels. The support package provided by MATLAB/Simulink can connect with Parrot Mambo Minidrone via Bluetooth 4.0, and access mini drone's internal sensor data and deploy the control algorithm in real time, the output of which will be sent back to MATLAB/Simulink and displayed on it. The sampling time of the mini drone control system is $T = 0.005$s, the position $[x,\ y,\ z]'$ and the attitude $[\phi, \theta, \psi]'$ of the minidrone are

Table 1
Parrot Minidrone parameters.

Variables	Values	Units
m_s	0.063	kg
l	0.108m	m
g	9.81	m/s^2
J_r	0.1021×10^{-6}	kgm^2
I_x	5.85×10^{-5}	kgm^2
I_y	7.17×10^{-5}	kgm^2
I_z	1×10^{-4}	kgm^2

Table 2
Design parameters of ESO UDSMC.

Variables	Values
$\omega_i (i = 1, 2)$	15
$\boldsymbol{\delta}_i (i = P, F, UN)$	$[0.8, 0.8]^T$
$\boldsymbol{C}_P$	diag$(0.5, 0.6, 0)$
$\boldsymbol{K}_{Pi} (i = 1, 2)$	diag$(-4, 6, 0)$
$\boldsymbol{C}_F$	diag$(3.6, 5, 0)$
$\boldsymbol{K}_{F1}$	diag$(4, 0.01)$
$\boldsymbol{K}_{F2}$	diag$(3, 0.008)$
$\boldsymbol{C}_{UN1}$	diag$(8m_s/\ u_1 cos\ \phi cos\ \psi, -8m_s/cos\ \psi u_1)$
$\boldsymbol{C}_{UN2}$	diag$(12m_s/\ u_1 cos\ \phi cos\ \psi, -12m_s/cos\ \psi u_1)$
$\boldsymbol{C}_{UN3}$	diag$(6, 6)$
$\boldsymbol{C}_{UN4}$	diag$(1, 1)$
$\boldsymbol{K}_{UN1}$	diag$(0.0002, 0.003)$
$\boldsymbol{K}_{UN2}$	diag$(0.001, 0.0015)$

estimated by the built-in sensor fusion algorithm based on Kalman filter; the linear velocity $[u,\ v,\ w]'$ and angular velocity $[p,\ q,\ r]'$ are calculated/estimated by ESO. The simulation package is performed on MATLAB/Simulink 2021a.

5.2. Experiment parameters

The initial position for quadrotor experiments is [0, 0, 0] m. Table 1 lists the variable values of Parrot Minidrone and Table 2 shows the UDSMC design parameters. The invariant controller in the outer loop is design as $G_{c1} = \frac{1}{0.01s^2+0.2s}$. The parameters of the PID controller are design as $K_P = \text{diag}[0.1, -0.1, 0.8, 0.003, 0.0024, 0.004]$, $K_I = \text{diag}[0.1, -0.1, 0.24, 0.006, 0.048, 0.002]$ and $K_D = \text{diag}[-0.2, 0.2, 0.5, 0.00012, 0.000096, 0.00012]$ for $[x,\ y,\ z, \phi, \theta, \psi]'$. The sliding mode controller design is followed by [36]. The sliding manifolds are designed as

$$\begin{cases} s_1 = c_z(z_d - z) + (\dot{z}_d - \dot{z}) \\ s_2 = c_\psi(\psi_d - \psi) + \left(\dot{\psi}_d - \dot{\psi}\right) \\ s_3 = c_1(\dot{x}_d - \dot{x}) + c_2(x_d - x) + c_3\left(\dot{\theta}_d - \dot{\theta}\right) + c_4(\theta_d - \theta) \\ s_4 = c_5(\dot{y}_d - \dot{y}) + c_6(y_d - y) + c_7\left(\dot{\phi}_d - \dot{\phi}\right) + c_8(\phi_d - \phi) \end{cases} \tag{57}$$

Table 3
Design parameters of SMC.

Variables	Values	Variables	Values
c_z	5	c_ψ	5
ε_1	0.8	ε_2	0.8
η_1	2	η_2	2
c_1	11	c_5	11
c_2	6	c_6	6
c_3	1	c_7	1
c_4	6	c_8	5
ε_3	−0.2	ε_4	0.2
η_3	−1.5	η_4	1.5

and its controllers are designed as

$$\begin{cases} u_1 = m_s \frac{c_z(\dot{z}_d - \dot{z}) + \ddot{z}_d + g + \varepsilon_1 \mathrm{sgn}(s_1) + \eta_1 s_1}{cos\phi cos\theta} \\ u_2 = \frac{I_x}{l}\left(\frac{c_5}{c_7}(\ddot{y}_d - \ddot{y}) + \frac{c_6}{c_7}(\dot{y}_d - \dot{y}) + \ddot{\phi}_d + \frac{c_8}{c_7}\left(\dot{\phi}_d - \dot{\phi}\right) + \frac{1}{c_7}(\varepsilon_4 \mathrm{sgn}(s_4) + \eta_4 s_4)\right) \\ u_3 = \frac{I_y}{l}\left(\frac{c_1}{c_3}(\ddot{x}_d - \ddot{x}) + \frac{c_2}{c_3}(\dot{x}_d - \dot{x}) + \ddot{\theta}_d + \frac{c_4}{c_3}\left(\dot{\theta}_d - \dot{\theta}\right) + \frac{1}{c_3}(\varepsilon_3 \mathrm{sgn}(s_3) + \eta_3 s_3)\right) \\ u_4 = I_z\left(c_\psi\left(\dot{\psi}_d - \dot{\psi}\right) + \ddot{\psi}_d + \varepsilon_2 \mathrm{sgn}(s_2) + \eta_2 s_2\right) \end{cases} \tag{58}$$

The related controller parameters are listed in Table 3.

5.3. Experiment results

In this experiment, the sampling time of the sensor and flight control system in quadrotor is 5 ms, which means that every 5 milliseconds, Parrot quadrotor reads and processes sensor data. Compared to the 1 ms sampling time in [37] (the latest real-time quadrotor control research), this experiment is more challenging and requires higher-quality controllers. The position tracking control performance of Parrot Minidrone is tested and evaluated by following the desired linear and spiral path. The quadrotor takes off from the ground, first quickly climbs to a height of 1 m, then follows the trajectory from (0,0) to (0,0.5) to (1,0.5) and finally reaches the (1,1) position according to the specified linear trajectory at 40 s. After this, quadrotor climbs to a height of 1.5 m at a steady speed in 20 s, and hovers at a height of 1.5 m for 20 s. At the same time, during the climbing and hovering process, the aircraft makes a circular motion with a radius of 30 cm.

The practical trajectory of the Parrot Minidrone is shown in Fig. 6 and Fig. 7. The further analysis of the tracking results is shown in Fig. 8, it shows the practical position tracking results of the quadrotor in each axis. To compare the tracking results for these three controllers numerically, the RMS values of the tracking errors are introduced as $e_{RMS} = \sqrt{\frac{1}{n}(e_1^2 + e_2^2 + \ldots + e_n^2)}$ with n being the total sampling size, the results are shown in Table 4. Intuitively, From Table 4 and Fig. 8, both the proposed ESO UDSM controller and the built-in PID controller can drive the quadrotor tracking the desired trajectory. And the more stable trajectory, less tracking error and faster response speed with the proposed controller than the PID controller in each channel can be observed. This shows that the proposed control algorithm is superior to the control algorithm that comes with the Parrot Minidrone product. Meanwhile, from Table 4, the proposed UDSMC is only slightly better than SMC, but UDSMC does not exhibit large overshoot in the XY axis and less chattering in the Z axis

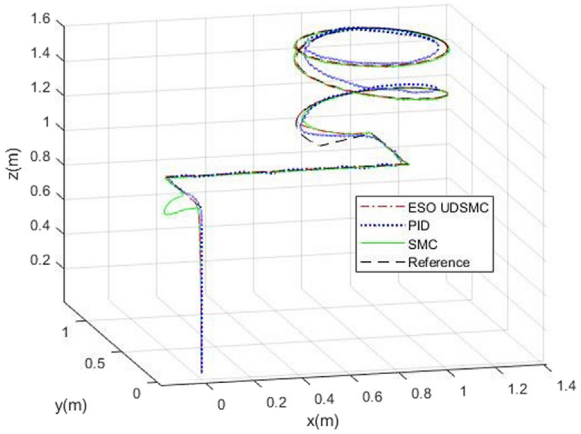

Fig. 6. Actual flight and desired trajectory in 3-D space. (For interpretation of the references to colour in this figure legend, the reader is referred to the web version of this article.)

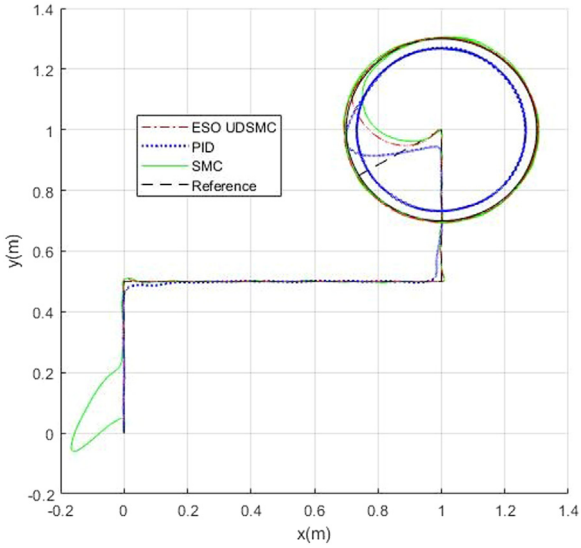

Fig. 7. Actual flight and desired trajectory in horizontal plane. (For interpretation of the references to colour in this figure legend, the reader is referred to the web version of this article.)

Table 4
RMS results for trajectory tracking.

	PID	ESO UDSMC	SMC
x(m)	0.0827	0.0302	0.0376
y(m)	0.0780	0.0114	0.0218
z(m)	0.0679	0.0674	0.0691

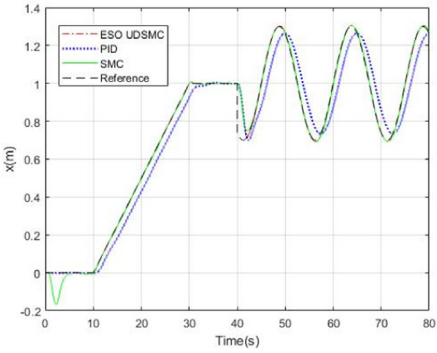

(a) x position tracking

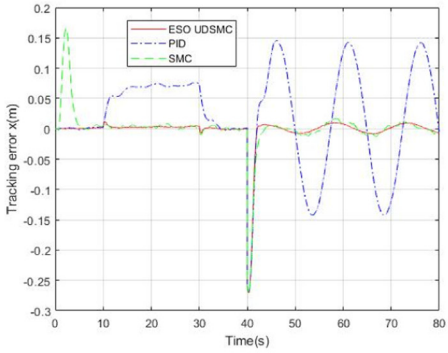

(b) Tracking error in x

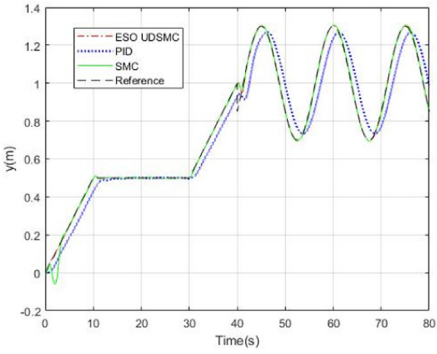

(c) y position tracking

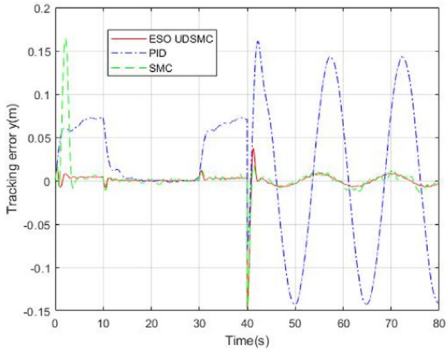

(d) Tracking error in y

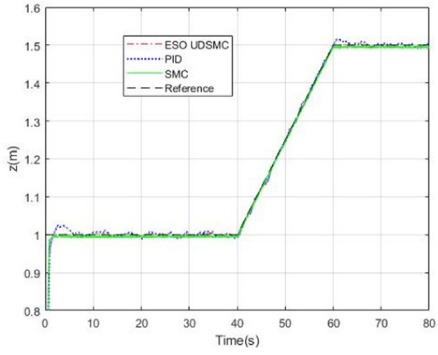

(e) z position tracking

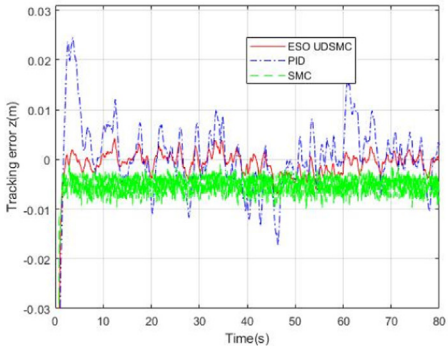

(f) Tracking error in z

Fig. 8. Actual trajectory tracking results.

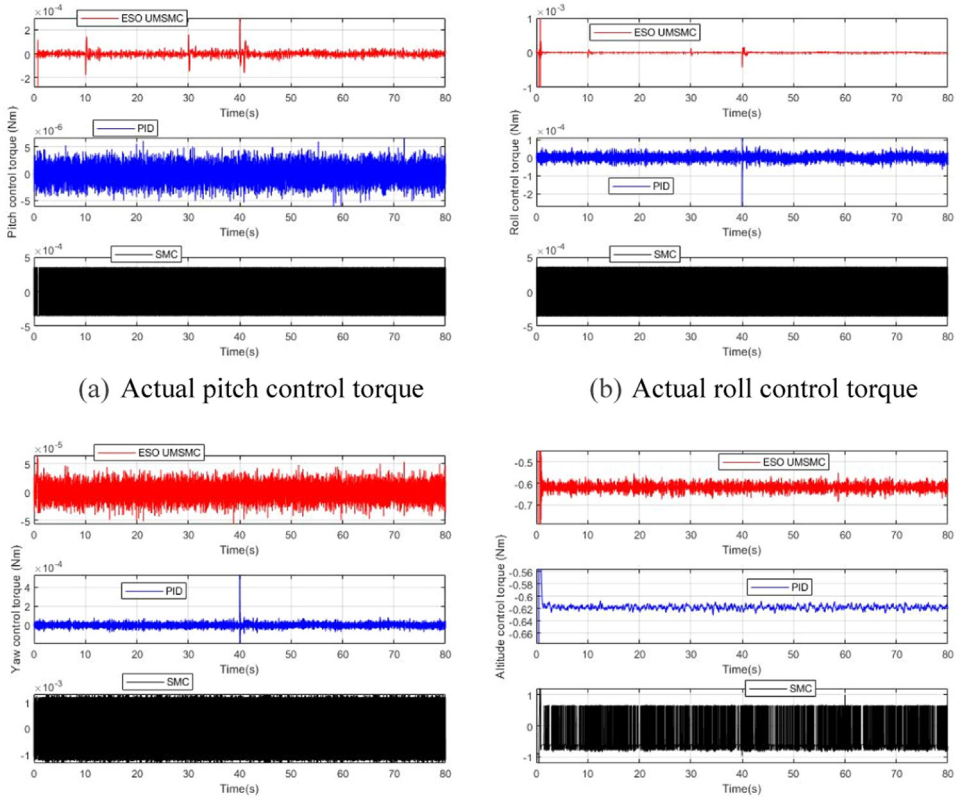

Fig. 9. control inputs results.

Table 5
RMS results for control inputs.

Channel	PID	UDSMC	SMC
Pitch control torque (N · m)	1.5748×10^{-6}	2.4246×10^{-5}	3.5199×10^{-4}
Roll control torque (N · m)	1.7226×10^{-5}	3.0336×10^{-5}	3.5850×10^{-4}
Yaw control torque (N · m)	2.3294×10^{-5}	1.3768×10^{-5}	0.0011
Altitude control thrust (N)	0.6189	0.6223	0.6749

(Fig. 8). This shows that the proposed algorithm still has certain advantages compared with advanced control algorithms.

Fig. 9 presents the control inputs for involved three controllers and the RMS ($u_{RMS} = \sqrt{\frac{1}{n}(u_1^2 + u_2^2 + \ldots + u_n^2)}$) results are shown in Table 5. The huge difference in control input chattering can be clearly observed in Fig. 9(d). From Table 4, frequent switching function triggers make large control input energy of SMC. Compared with PID, the proposed UDMSC has a larger control input energy, but within the acceptable range. Therefore, considering the superior control performance of the proposed controller, although it has obvious fluctuations

and higher control input energy, the implementation of ESO UDMSC on quadrotor can be successful.

Remark 9. It should be noted that the performance of the built-in PID controller could be improved after careful tuning. However, this is very empirical and the original parameters for PID controller are not changed in this experiment. From Fig. 9, the chattering problems appears in both UDSMC and SMC in this experiment because of the frequent switching operations due to long sampling time. Saturation function can reduce chattering but may result in the decrease of the robustness and tracking performance.

Remark 10. Although these advanced control algorithms can achieve better control performance, however, in real-time applications, considering the computational cost, hardware sampling time, and unpredictable changes in external environmental factors, PID is still a mature controller that cannot be completely replaced.

6. Conclusions

This study proposes a robust control strategy for quadrotor trajectory tracking based on the ESO UDSMC method. Compared with the built-in PID and SMC based flight control system of the Parrot Minidrone, the proposed control strategy not only achieves the fast response of the quadrotor control system, but also guarantees flight stability and efficient desired flight trajectories tracking performance without offline identification of the quadrotor dynamic system. At the same time, the 5 ms system sampling time also makes the designed control system have a large room for improvement with advanced computational algorithms for most quadrotors.

However, because of the small size, lightweight and low motor torque of the Parrot Minidrone quadrotor used in the experiment, which cannot conduct flight tests in long-distance flights or complex environments. Also, this experiment does not involve variable load and unpredictable wind disturbance (indoor experiment). One of the future works will evaluate the proposed controller for stable flight under unknown wind disturbance. It is believed that with the improvement of UAV hardware support, the proposed quadrotor control system can reach better control performance.

Funding

This research received no external funding.

Declaration of competing interest

The authors declare that they have no known competing financial interests or personal relationships that could have appeared to influence the work reported in this paper.

Acknowledgements

The authors express their gratitude to the editors and the anonymous reviewers for their helpful comments and constructive suggestions about the revision of the paper. The first author is acknowledging the partial PhD studentship for the research project from the University of the West England, Bristol.

References

[1] L. Besnard, Y.B. Shtessel, B. Landrum, Quadrotor vehicle control via sliding mode controller driven by sliding mode disturbance observer, J. Franklin Inst. 349 (2) (2012) 658–684.

[2] A. Tayebi, S. McGilvray, Attitude stabilization of a VTOL quadrotor aircraft, IEEE Trans. Control Syst. Technol. 14 (3) (2006) 562–571.

[3] H. Shakhatreh, A.H. Sawalmeh, A. Al-Fuqaha, Z. Dou, E. Almaita, I. Khalil, ... M. Guizani, Unmanned aerial vehicles (UAVs): a survey on civil applications and key research challenges, Ieee Access, 7, 2019, pp. 48572–48634.

[4] R. López-Gutiérrez, A.E. Rodriguez-Mata, S. Salazar, I. González-Hernández, R. Lozano, Robust quadrotor control: attitude and altitude real-time results, J. Intell. Robotic Syst. 88 (2) (2017) 299–312.

[5] H. Liu, J. Xi, Y. Zhong, Robust attitude stabilization for nonlinear quadrotor systems with uncertainties and delays, IEEE Trans. Ind. Electron. 64 (7) (2017) 5585–5594.

[6] X. Xiang, C. Liu, H. Su, Q. Zhang, On decentralized adaptive full-order sliding mode control of multiple UAVs, ISA Trans. 71 (2017) 196–205.

[7] B. Panomrattanarug, K. Higuchi, F. Mora-Camino, Attitude control of a quadrotor aircraft using LQR state feedback controller with full order state observer, in: The SICE Annual Conference 2013, IEEE, 2013, September, pp. 2041–2046.

[8] Szafranski, G., & Czyba, R. (2011). Different approaches of PID control UAV type quadrotor.

[9] L. Martins, C. Cardeira, P. Oliveira, Linear quadratic regulator for trajectory tracking of a quadrotor, IFAC-PapersOnLine 52 (12) (2019) 176–181.

[10] J.J.E. Slotine, W. Li, Applied Nonlinear Control, 199, Prentice hall, Englewood Cliffs, NJ, 1991, p. 705.

[11] J.J. Xiong, E.H. Zheng, Position and attitude tracking control for a quadrotor UAV, ISA Trans. 53 (3) (2014) 725–731.

[12] K.P.B. Chandra, H. Alwi, C. Edwards, Fault reconstruction for a quadrotor using an lpv sliding mode observer1, IFAC-PapersOnLine 48 (21) (2015) 374–379.

[13] T. Huang, D. Huang, Z. Wang, X. Dai, A. Shah, Generic adaptive sliding mode control for a quadrotor UAV system subject to severe parametric uncertainties and fully unknown external disturbance, Int. J. Control Automat. Syst. 19 (2) (2021) 698–711.

[14] J.J. Xiong, G. Zhang, Discrete-time sliding mode control for a quadrotor UAV, Optik (Stuttg) 127 (8) (2016) 3718–3722.

[15] O. Mofid, S. Mobayen, Adaptive sliding mode control for finite-time stability of quad-rotor UAVs with parametric uncertainties, ISA Trans. 72 (2018) 1–14.

[16] K. Zhang, Y. Shi, H. Sheng, Robust nonlinear model predictive control based visual servoing of quadrotor UAVs, IEEE/ASME Trans. Mechatron. 26 (2) (2021) 700–708.

[17] N. Xie, Y. Yu, C. Sun, An image-based decoupling controller of quadrotor for moving target tracking, J. Control Decis. (2022) 1–12.

[18] X. Lin, Y. Yu, C.Y. Sun, A decoupling control for quadrotor UAV using dynamic surface control and sliding mode disturbance observer, Nonlinear Dyn. 97 (1) (2019) 781–795.

[19] K. Gamagedara, T. Lee, Geometric adaptive controls of a quadrotor unmanned aerial vehicle with decoupled attitude dynamics, J. Dyn. Syst. Meas. Control 144 (3) (2022).

[20] C. Huang, Design of decoupling fuzzy logic controller for quadrotor UAV, in: Journal of Physics: Conference Series, 1684, IOP Publishing, 2020, November.

[21] X. Cheng, Z.W. Liu, Robust tracking control of a quadcopter via terminal sliding mode control based on finite-time disturbance observer, in: 2019 14th IEEE Conference on Industrial Electronics and Applications (ICIEA), IEEE, 2019, June, pp. 1217–1222.

[22] A. Eskandarpour, I. Sharf, A constrained error-based MPC for path following of quadrotor with stability analysis, Nonlinear Dyn. 99 (2) (2020) 899–918.

[23] R. Falcón, H. Ríos, A. Dzul, Comparative analysis of continuous sliding-modes control strategies for quad-rotor robust tracking, Control Eng. Pract. 90 (2019) 241–256.

[24] O. Mofid, S. Mobayen, C. Zhang, B. Esakki, Desired tracking of delayed quadrotor UAV under model uncertainty and wind disturbance using adaptive super-twisting terminal sliding mode control, ISA Trans. 123 (2022) 455–471.

[25] H. Hassani, A. Mansouri, A. Ahaitouf, Robust autonomous flight for quadrotor UAV based on adaptive nonsingular fast terminal sliding mode control, Int. J. Dyn. Control 9 (2) (2021) 619–635.

[26] R. Falcón, H. Ríos, A. Dzul, Comparative analysis of continuous sliding-modes control strategies for quad-rotor robust tracking, Control Eng. Pract. (2019) 90, 241-256xxxx.
[27] C. Greatwood, A.G. Richards, Reinforcement learning and model predictive control for robust embedded quadrotor guidance and control, Auton. Robots 43 (7) (2019) 1681–1693.
[28] V. Nekoukar, N.M. Dehkordi, Robust path tracking of a quadrotor using adaptive fuzzy terminal sliding mode control, Control Eng. Pract. 110 (2021) 104763.
[29] Q. Zhu, R. Li, X. Yan, U-model-based double sliding mode control (UDSM-control) of nonlinear dynamic systems, Int. J. Syst. Sci. 53 (6) (2022) 1153–1169.
[30] J. Ajmera, V. Sankaranarayanan, Point-to-point control of a quadrotor: theory and experiment, IFAC-PapersOnLine 49 (1) (2016) 401–406.
[31] B.Z. Guo, Z.L. Zhao, On the convergence of an extended state observer for nonlinear systems with uncertainty, Syst. Control Lett. 60 (6) (2011) 420–430.
[32] R. Li, Q. Zhu, J. Kiely, W. Zhang, Algorithms for U-model-based dynamic inversion (UM-dynamic inversion) for continuous time control systems, Complexity (2020) 2020.
[33] R. Li, Q. Zhu, J. Yang, P. Narayan, X. Yue, Disturbance-observer-based U-control (DOBUC) for nonlinear dynamic systems, Entropy 23 (12) (2021) 1625.
[34] R. Li, Q. Zhu, W. Zhang, X. Yue, P. Narayan, An improved U-control design for nonlinear systems represented by input/output differential models with disturbance observer, Int. J. Control (2022) 1–34 (just-accepted).
[35] R. Li, Q. Zhu, P. Narayan, A. Yue, Y. Yao, M. Deng, U-model-based two-degree-of-freedom internal model control of nonlinear dynamic systems, Entropy 23 (2) (2021) 169.
[36] E.H. Zheng, J.J. Xiong, J.L. Luo, Second order sliding mode control for a quadrotor UAV, ISA Trans. 53 (4) (2014) 1350–1356.
[37] L. Chen, Z. Liu, H. Gao, G. Wang, Robust adaptive recursive sliding mode attitude control for a quadrotor with unknown disturbances, ISA Trans. 122 (2022) 114–125.